ACS Infectious Diseases

pubs.acs.org/journal/aidcbc

Article

Toward Catalytic Antibiotics: Redesign of Fluoroquinolones to Catalytically Fragment Chromosomal DNA

Moshe N. Goldmeier, Sofya Katz, Fabian Glaser, Valery Belakhov, Alina Khononov, and Timor Baasov*

Cite This: *ACS Infect. Dis.* 2021, 7, 608−623

Read Online

ACCESS | Metrics & More | Article Recommendations | Supporting Information

ABSTRACT: A library of ciprofloxacin−nuclease conjugates was designed and synthesized to investigate their potential as catalytic antibiotics. The Cu(II) complexes of the new designer compounds (i) showed excellent *in vitro* hydrolytic and oxidative DNase activity, (ii) showed good antibacterial activity against both Gram-negative and Gram-positive bacteria, and (iii) proved to be highly potent bacterial DNA gyrase inhibitors via a mechanism that involves stabilization of the fluoroquinolone−topoisomerase−DNA ternary complex. Furthermore, the Cu(II) complexes of two of the new designer compounds were shown to fragment supercoiled plasmid DNA into linear DNA in the presence of DNA gyrase, demonstrating a "proof of concept" *in vitro*. These ciprofloxacin−nuclease conjugates can therefore serve as models with which to develop next-generation, *in vivo* functioning catalytic antimicrobials.

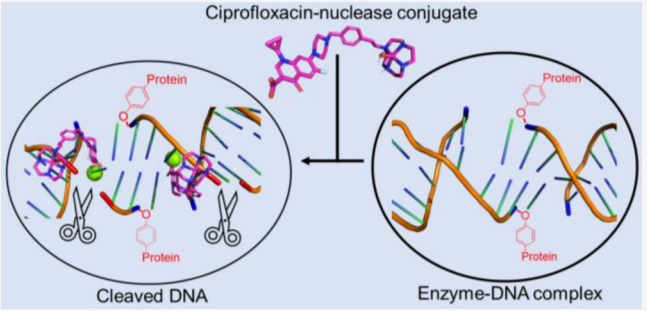

KEYWORDS: *fluoroquinolone, catalytic antibiotic, DNA cleavage, antimicrobial resistance, metallodrugs, cyclen*

Fluoroquinolones are highly potent, broad spectrum antibiotics that are among the most commonly prescribed antibacterials in the world.[1] They exert a bacteriostatic effect by selectively binding to the bacterial topoisomerase IIA−DNA complex and thereby inhibiting DNA replication. At higher doses (5−10 × minimum inhibitory concentration (MIC)), they exert a bactericidal effect by causing fragmentation of the bacterial chromosome, which is toxic for the bacteria.[2] However, the emergence of resistance is becoming a critical issue that is limiting the use of this class of antibiotics.[3] Consequently, several novel bacterial topoisomerase type IIA inhibitors have been developed that retain potency against quinolone-resistance bacterial strains by offering an alternative binding mode or mechanism of action, including among others NXL101 and REDX07638.[4]

Unfortunately, however, it has been well documented that once a new antibiotic is introduced into the clinic, whether it is a novel chemical entity acting at a distinct bacterial target or a semisynthetic derivative that counters the resistance to its parent drug, it is only a short matter of time until new resistance will yet again emerge and create a public health problem.[5] Consequently, it would seem apparent that changing the mechanism of inhibition or binding mode at the target does not necessarily address the fundamental problem of delaying resistance development; it simply "buys more time" for the topoisomerase targeting antibacterials. The significance of this health problem has re-energized the search for novel approaches that would allow humans to stay more than one step ahead.

One innovative approach is the development of catalytic antibiotics as small molecule-based therapeutic agents to mediate catalytic inactivation of a specific bacterial target to form an inactive or dysfunctional entity. Inhibition occurs in at least two steps and in a manner analogous to the Michaelis−Menten enzyme model: The compound must first bind noncovalently to the target; the resulting complex then undergoes specific chemical modification, which results in the deleterious transformation of the target and the release of the drug for another cycle (Figure 1).[6−8] Thus, unlike conventional antibiotics that inhibit their targets by either noncovalent or covalent interactions, catalytic antibiotics should promote multiple turnovers of a catalytic cycle. There are many advantages to this approach, including improved potency and lower toxicity (due to lower dosage requirements) and general applicability to targets with weak binding sites.[6,7] Furthermore, this approach is likely to delay resistance for two reasons. First, individual target-based resistance mutations are unlikely to affect the k_2 rate constant even if they do affect the rate at which the inhibited complex forms (K_i). In other words, catalytic antibiotics would be able to target mutants that have

Received: November 4, 2020
Published: January 15, 2021

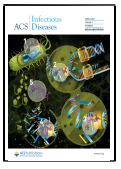

https://dx.doi.org/10.1021/acsinfecdis.0c00777
ACS Infect. Dis. 2021, 7, 608−623

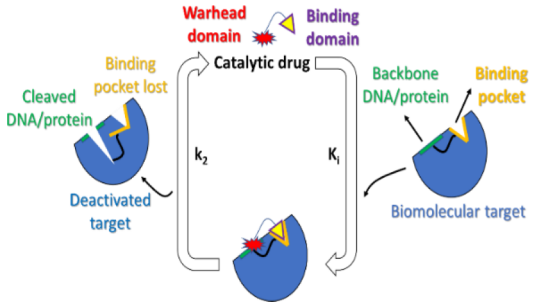

Figure 1. General scheme representing the mechanism for catalytic deactivation of biomolecular target.

acquired energetically "shallow" binding sites to the pharmacophore scaffold, since the efficiency of such enzymatic systems is governed by the ratio of these two parameters and not just by K_i.[7] Thus, given enough exposure to the compound, even mutants that react considerably more slowly will become deactivated and so resistance is likely to develop more slowly. Second, the killing activity of catalytic antibiotics is expected to be totally independent of cellular processes such as protein synthesis or anaerobic conditions. Such a feature could be particularly important with pathogens such as *Mycobacterium tuberculosis* that enter a dormant state in which they become tolerant to many antimicrobials.[2]

In the past few decades, artificial enzymes that target nucleic acids or proteins have been well studied.[6,9] However, in most cases, the reported catalysts suffer from a lack of substrate selectivity, which can lead to lower catalyst efficiency, side effects, and toxicity.[6] One approach to addressing this issue is to join a substrate selective binding motif to the catalytic warhead (Figure 1).[6] Several studies have recently reported on multifunctional antibacterial metallopeptides that modify nucleic acids, proteins, or phospholipids via ROS generated by an amino terminal copper and nickel (ATCUN) binding motif. For example, Cowan and co-workers reported on the conjugates of Cu(II)-ATCUN with known antimicrobial peptides[10,11] and demonstrated significant improvement in antibacterial activity relative to parent peptides. These seminal works by Cowan's laboratory, along with those by Angeles-Boza's[12,13] and other laboratories[14] clearly show that the attachment of a metal-binding motif can promote oxidative damage and enhance the antibacterial activity of known antibacterial peptides. However, the conservative[11,13] changes in MIC observed versus the parent peptides were not as high as would be expected from a catalytic metallodrug, which suggests that more advanced design strategies are needed to realize the full clinical potential of catalytic antibiotics.

To address this issue, we set out to explore catalytic antibiotics that are designed to cleave a specific, "critical" chemical bond in a bacterial target that is projected to result in the immediate deactivation of the target. In our previous work,[15] we synthesized and evaluated new variants of an aminoglycoside antibiotic that would selectively and catalytically act on the bacterial ribosome to irreversibly deactivate it via metal-free, hydrolytic RNase activity. We demonstrated that an appropriately designed aminoglycoside variant has the capacity to bind selectively to the parent aminoglycoside binding site and to induce the conformational changes that are necessary to lower the activation barrier of the transition state for hydrolytic cleavage.

Herein, we focus on redesigning ciprofloxacin to catalytically cleave a specific scissile phosphodiester bond at the site of the fluoroquinolone–topoisomerase–DNA ternary complex, where the bound DNA is (a) stretched[16] and (b) free of significant binding interactions with the surrounding residues (Figure 2).

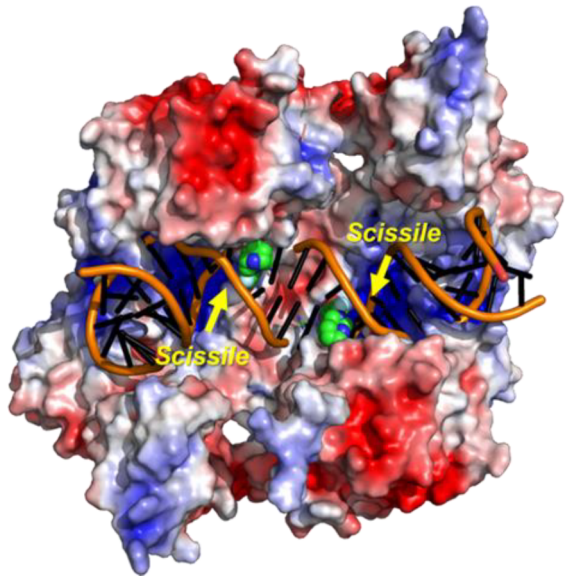

Figure 2. Three-dimensional representation of the ternary complex as obtained from an X-ray crystal structure (PDB ID code 2XKK[17]). The ParE28–ParC58 fusion truncate of *Acinetobacter baumannii* topoisomerase IV (Topo IV) shown as an electrostatic potential map (blue = positive, red = negative) in complex with the fluoroquinolone moxifloxacin (shown as spheres; carbon = green, nitrogen = blue) and DNA (shown as orange/black cartoon); image generated using PyMOL.[18] The yellow arrows mark out the scissile phosphodiester bonds adjacent to the fluoroquinolone molecules.

This has the potential to (i) irreversibly deactivate the enzyme target, (ii) fragment the chromosome, and most crucially (iii) also interfere with the affinity of the binding moiety to the target such that a catalytic cycle is generated, as shown in Figure 1. With this premise, we decided to assemble an initial library of ciprofloxacin–nuclease conjugates and to investigate their potential as catalytic antibiotics. The Cu(II) complexes of the new designer compounds (i) showed excellent *in vitro* hydrolytic and oxidative DNase activity, (ii) showed good antibacterial activity against both Gram-negative and Gram-positive bacteria, and (iii) proved to be highly potent bacterial DNA gyrase inhibitors via a mechanism that involves stabilization of the ternary complex. Furthermore, the Cu(II) complexes of two of the new designer compounds were shown to fragment supercoiled plasmid DNA into linear DNA in the presence of DNA gyrase, demonstrating a "proof of concept" *in vitro*.

RESULTS AND DISCUSSION

Design Hypothesis. We primarily considered the following three key aspects: (i) the choice of "catalytic warhead" that efficiently cleaves the DNA substrate, (ii) the choice of attachment site of a catalytic warhead on the ciprofloxacin scaffold, and (iii) the linker structure that connects ciprofloxacin to the catalytic warhead.

https://dx.doi.org/10.1021/acsinfecdis.0c00777
ACS Infect. Dis. 2021, 7, 608–623

(i) The Choice of Catalytic Warhead. Phosphodiester bonds are extremely stable toward hydrolysis: the half-life for hydrolysis of phosphodiester bonds in DNA at neutral pH and 25 °C is estimated to be 16 million years.[19] Despite such unique stability, natural nuclease enzymes cleave DNA very efficiently providing impressive rate acceleration.[20]

For most natural metallic nucleases, magnesium is the metal of choice, while in a few other cases divalent Zn or Ca are used.[21] Inspired by natural metallonucleases, numerous studies have reported on the design of strongly Lewis acidic metal complexes that promote hydrolysis of the DNA phosphodiester backbone.[22] Although very efficient, metal-independent natural nucleases exist, artificial nonmetallic hydrolytic DNA cleavage remains a challenge, and the rate enhancements of reported compounds are generally not as good as those of metal-containing systems[23] (Figure 3).

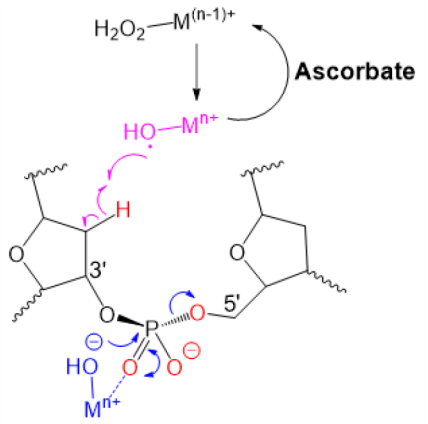

Figure 3. Hydrolytic (blue arrows) and oxidative (purple arrows) DNA cleavage pathways.

An alternative approach is to use redox active metals that efficiently cleave DNA in the presence of an oxidant (H_2O_2 or O_2) and endogenous reductant (e.g., ascorbic acid), by generating ROS such as the hydroxyl radical, which typically abstract hydrogen from the deoxyribose ring followed by spontaneous cleavage of C−C and C−O bonds[22] (Figure 3).

In both these approaches, it is essential that the metal−ligand complex is highly stable, since both prokaryotic and eukaryotic cells have sophisticated acquisition systems to scavenge essential metals from their environment, as an imbalance in metal homeostasis is deleterious.[24]

Taking into account the above considerations, we selected 1,4,7,10-tetraazacyclododecane (cyclen) as a scaffold and Cu(II)-cyclen and Co(III)-cyclen as the nuclease warheads in our designer structures. Cu(II)-cyclen is thermodynamically very stable[25] and cleaves DNA primarily by metal-bound ROS in the presence of redox adjuvants.[26] Although Cu(II)-cyclen itself has poor nuclease activity in the absence of adjuvants,[27] we anticipated that in our system, the Cu(II)-cyclen warhead connected with a spacer to ciprofloxacin might show enhanced hydrolytic or oxidative activity (compared to Cu(II)-cyclen alone) due to the proximity effect (or its increased effective molarity[28]). Co(III)-cyclen is expected to be even more thermodynamically stable in view of the exchange-inertness of Co(III)[29,30] and is more active than the Cu(II)-cyclen in the absence of adjuvants via a hydrolytic pathway.[27] It is important to note, however, that the greater electrostatic charge of Co(III) may also enhance the binding of the metal complex to the DNA and it is difficult to predict how exactly this would affect the rate of the catalytic turnover.[27]

The Choice of (ii) Attachment Site of a Catalytic Warhead and (iii) the Linker Structure. Previous studies on SAR of fluoroquinolones have demonstrated a high tolerance for structural variations at the 7-position of the phenyl ring[31,32] (Figure 4). This phenomenon can be rationalized by the

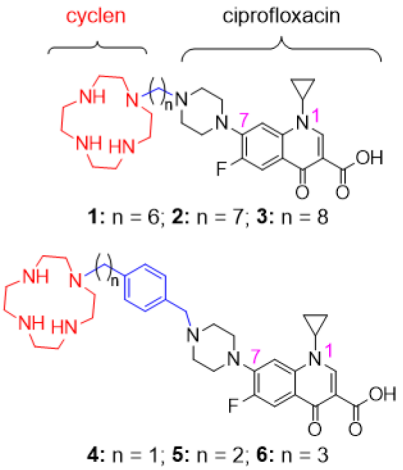

Figure 4. Designed structures **1**−**6** as derivatives of ciprofloxacin.

structural information available; the bulky substituent at the 7-position is seen to project into a large,[17] solvent-accessible volume of space above the cleaved DNA.

For these reasons, we chose to modify ciprofloxacin at the terminal nitrogen of the piperazine moiety. We reasoned that the catalytic warhead should be joined to the piperazine component via a hydrophobic linker to avoid off-target polar interactions between the linker and the surrounding amino acid residues. Additionally, we chose to vary the length and flexibility (aliphatic vs aromatic) of the linker to explore a wide array of attack trajectories toward the scissile DNA phosphodiester bond, since in order to facilitate hydrolytic DNA cleavage one of the cyclen N−$H^{\delta+}$ bonds needs to be suitably positioned to provide the necessary phosphate stabilization as a hydrogen bond donor while the metal-activated nucleophile (water) must be well orientated for an in-line nucleophilic attack[33] (Figure 5). These design principles were then used together with molecular docking (Autodock 4.2[34] and Ledock;[35] see Supporting Information for details) to design the new derivatives of ciprofloxacin, compounds **1**−**6** (Figure 4). The cyclen warhead is connected to ciprofloxacin via an aliphatic spacer in compounds **1**−**3** and via an aromatic spacer in compounds **4**−**6**. The docking data (data not shown) for all the Cu(II) and Co(III) complexes of **1**−**6** predict that (i) the ciprofloxacin scaffold will bind in the native pocket and (ii) the cyclen warhead will be brought into very close proximity to the DNA. Interestingly, both software packages predict that **5**-Cu(II) and **5**-Co(III) are the most likely complexes to be capable of hydrolytic DNA cleavage (Figure 5).

Synthesis of 1−6 and Their Cu(II) and Co(III) Complexes. Compounds **1**−**6** were synthesized in five or six chemical steps, as detailed in Scheme 1. First, commercially available ciprofloxacin was ester-protected under acidic conditions to give methyl ester **7**. Compound **7** was then

https://dx.doi.org/10.1021/acsinfecdis.0c00777
ACS Infect. Dis. 2021, 7, 608−623

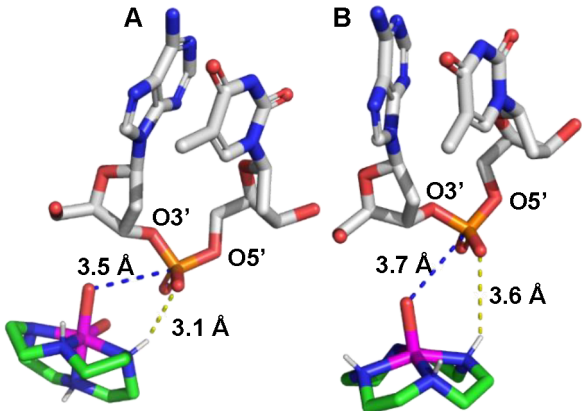

Figure 5. Docking pose of energy minimum of low energy cluster for 5-Co(III) (A) and 5-Cu(II) (B) in crystal structure 2XKK.[17] For clarity, only the metal−cyclen warhead and the adjacent DNA residues are shown (green carbons = cyclen, white carbons = DNA, metal = magenta). Blue dashed lines indicate distance between metal-activated water and scissile phosphodiester bond. Yellow dashed lines indicate electrostatic interaction between phosphate oxygen and N−$H^{\delta+}$.

treated with an excess of the relevant dibromo compound under basic conditions to afford compounds **8a−f** containing a terminal bromide. It is notable that while the majority of the dibromo compounds used here are commercially available, the dibromo derivatives 1-(2-bromoethyl)-4-(bromomethyl) benzene (**10**) and 1-(bromomethyl)-4-(3-bromopropyl) benzene (**11**) required for preparing **8e** and **8f** are not commercially available. Therefore, **10** and **11** were synthesized from commercially available starting materials in two and four steps, respectively, as detailed in Supplementary Scheme S1.

Initially, the bromide **8a** was treated with tri-Boc-cyclen[36] under basic conditions in an attempt at preparing pure **9a** in one step. However, the reaction did not proceed even after being heated at high temperature for a long time. These conditions were only successful for the preparation of **9d**. For the rest of the compounds, instead of using tri-Boc-cyclen, the bromo derivative was first treated with free cyclen[37] under base conditions followed by Boc-protection of the remaining secondary amines to yield the corresponding tri-Boc protected derivatives. For example, compound **8a** was first coupled to free cyclen under basic conditions (Cs_2CO_3, CH_3CN) and then Boc-protected and finally **9a** was isolated using column chromatography. Thus, **9b,c** and **9e,f** were synthesized via cyclen as described for **9a**.

Finally, compounds **9a−f** were treated sequentially with strong base (LiOH) and then strong acid (TFA) to remove the ester and Boc protecting groups. Compounds **1−6** were then converted to the free amine form using an Amberlite ion-exchange column. The final **1−6** structures were characterized by NMR and MS techniques.

The ligands **1−6** were treated with aqueous Cu(II) chloride to afford the corresponding monoaqua Cu(II) complexes. The complexes were characterized by UV−vis, EPR, and HMRS (see Methods for details). The aqua-hydroxo Co(III) complexes of **1−6** were prepared in three steps according to the reported literature.[38] The initial Co(III)-CO_3 complexes were characterized by MS, UV−vis, and ^{13}C NMR, the intermediate Co(III)-Cl_2 complexes were characterized by UV−vis and HRMS and the aqua-hydroxo-Co(III) complexes were characterized by UV−vis (see Supporting Information for details).

DNA Cleavage Assays. To evaluate the biologically pertinent nuclease activity of Cu(II) and Co(III) complexes of **1−6**, assays were performed (a) in the absence of redox adjuvants and also (b) in the presence of 0.32 mM ascorbic acid (for the Cu(II) complexes), since its (eukaryotic) intracellular concentration is also in this range.[39,40] Agarose

Scheme 1. Synthesis of Ligands 1−6[a]

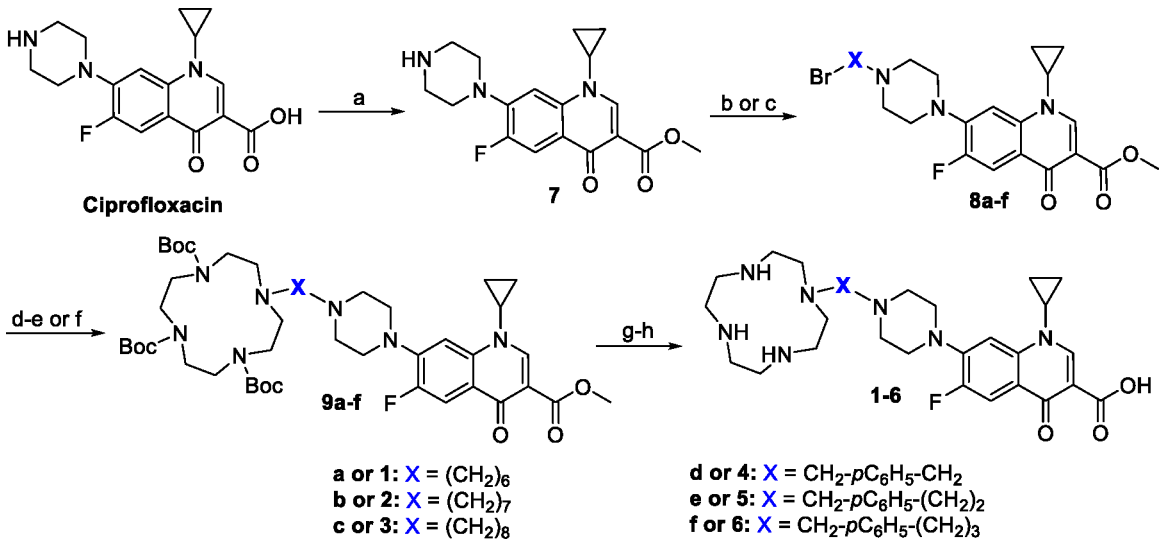

[a]Reagents and conditions: (a) Dowex 50WX8, MeOH, reflux, 81%; (b) DIPEA, CH_3CN, 60 °C, $Br(CH_2)_6Br$, 54% (**8a**), $Br(CH_2)_7Br$, 61% (**8b**), $Br(CH_2)_8Br$, 58% (**8c**), 1,4-bis(bromomethyl)-benzene, 22% (**8d**); (c) DIPEA, CH_3CN, 0 °C to rt,1-(2-bromoethyl)-4-(bromomethyl)benzene, 60% (**8e**), 1-(bromomethyl)-4-(3-bromopropyl)-benzene, 63% (**8f**); (d) cyclen, Cs_2CO_3, CH_3CN, 60 °C; (e) Boc_2O, Et_3N, DCM, 0 °C to rt, 45% over 2 steps (**9a**), 33% over 2 steps (**9b**), 49% over 2 steps (**9c**), 34% over 2 steps (**9e**), 55% over 2 steps (**9f**); (f) triBoc-cyclen, DIPEA, DCM, rt, 72% (**9d**); (g) LiOH, MeOH/H_2O 5:1, rt; (h) TFA, DCM, rt, Amberlite, 48% over 2 steps (**1**), 49% over 2 steps (**2**), 61% over 2 steps (**3**), 51% over 2 steps (**4**), 38% over 2 steps (**5**), 59% over 2 steps (**6**).

https://dx.doi.org/10.1021/acsinfecdis.0c00777
ACS Infect. Dis. 2021, 7, 608−623

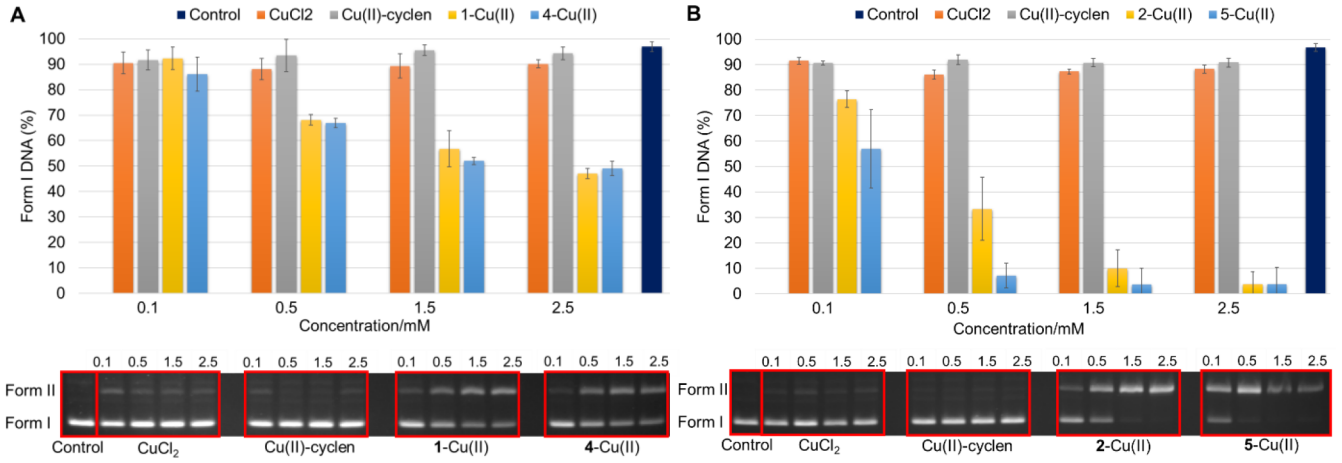

Figure 6. Comparative concentration dependent cleavage of (+) supercoiled pHOT-1 plasmid (0.007 $\mu g\ \mu L^{-1}$) in HEPES buffer (50 mM, pH 7.4) over 5 h. Standard deviations of three independent experiments are shown as error bars for Cu(II) alone ($CuCl_2$) and its complexes with cyclen, **1** and **4** (A), or **2** and **5** (B). The agarose gel images show one representative experiment.

gel electrophoresis (1% agarose) and ethidium bromide staining was used to monitor the conversion of supercoiled (form I) pHOT-1 plasmid DNA into its nicked form (form II) or into multiply nicked DNA; no linear form (form III) was observed. Comparative DNA cleavage experiments of the ligands **1**−**6** with and without the chelated metals clearly demonstrated that the cleavage activity of **1**−**6** without any metal could be excluded (Supplementary Figure S1). As reported previously, due to the presence of multiple positive charges in the ligands, it is necessary to use an ion-exchange based microscale procedure for removal of the ligands prior to electrophoresis (above a critical concentration; Supplementary Figure S2), as neutralization of the negatively charged DNA by these strongly bound ligands prevents the DNA from moving in the electric field.[27]

Cleavage Experiments in the Absence of Adjuvants: Cu(II) Complexes. As illustrated in Figure 6A, both the **1**-Cu(II) and **4**-Cu(II) complexes show very significant enhancement in the rates of DNA cleavage when compared with either $CuCl_2$ or Cu(II)-cyclen. Presumably, this enhancement is mediated by the extra binding affinity provided by the intercalating properties of the ciprofloxacin scaffold. Furthermore, both **2**-Cu(II) and **5**-Cu(II) complexes show significant cleavage enhancement even in relation to the activity of **1**-Cu(II) and **4**-Cu(II) (Figure 6B). Indeed, there appears to be a strong correlation between the linker length and the cleavage activity; **1**-Cu(II) and **4**-Cu(II) show similar activity and both have six atoms in the linker, while **2**-Cu(II) and **5**-Cu(II) also show similar activity and both have seven atoms in the linker. Surprisingly, **3**-Cu(II) and **6**-Cu(II), both of which contain eight atoms in the linker, showed only very limited activity (Supplementary Figure S3). The overall order of reactivity is therefore as follows: **2**-Cu(II) ≈ **5**-Cu(II) > **1**-Cu(II) ≈ **4**-Cu(II) ≫ **3**-Cu(II) ≈ **6**-Cu(II). In summary, these data demonstrate that the nuclease activity is very sensitive to the linker length between the Cu(II)-cyclen warhead and the ciprofloxacin scaffold.

To investigate the mechanism of cleavage, a scavenging assay was performed with hydroxyl radical scavengers (DMSO, *t*-BuOH, KI), a singlet oxygen scavenger (NaN_3), a superoxide scavenger (KI), and NaCl as a control for ionic strength (Figure 7). The data clearly rules out the involvement of the hydroxyl radical in the catalytic activity of **5**-Cu(II), since both

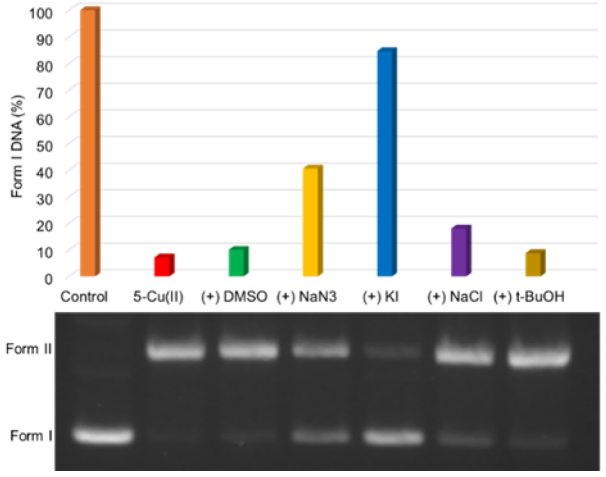

Figure 7. Cleavage of (+) supercoiled pHOT-1 plasmid (0.007 $\mu g\ \mu L^{-1}$) in HEPES buffer (50 mM, pH 7.4) with **5**-Cu(II) (0.5 mM) alone or with a series of scavenging compounds (10 mM), over 5 h.

DMSO and *t*-BuOH have no significant inhibitory effect. In stark contrast, KI and NaN_3 both have very significant inhibitory effect, while NaCl does not, ostensibly suggesting that both singlet oxygen and superoxide radicals contribute to the catalytic activity of **5**-Cu(II). Indeed, other studies have reported on similar copper complexes (bearing DNA intercalators) that cleave DNA via an oxidative pathway in the absence of adjuvants.[41,42] However, since the inhibitory effects of NaN_3 and KI could also be mediated by their ability to displace the copper-coordinated water, these data do not rule out the possibility that a hydrolytic mechanism contributes to the nuclease activity. Indeed, UV−vis spectroscopic analysis of the mixture of Cu(II)-cyclen with NaN_3, KI, or NaCl (Supplementary Figures S4−6) reveal that NaN_3 and KI displace the Cu(II) associated water while the NaCl does not (i.e., at the ratio used in the scavenging assay). Finally, the fact that one additional carbon in the linker can distinguish excellent nuclease activity enhancement (relative to Cu(II)-cyclen) from virtually no activity at all [i.e., **5**-Cu(II) and **2**-Cu(II) vs **3**-Cu(II) and **6**-Cu(II)] suggests that a hydrolytic mechanism contributes significantly to the nuclease activity of **1**-Cu(II), **2**-Cu(II), **4**-Cu(II), and **5**-Cu(II).

https://dx.doi.org/10.1021/acsinfecdis.0c00777
ACS Infect. Dis. 2021, 7, 608−623

Cleavage Experiments in the Absence of Adjuvants: Co(III) Complexes. The Co(III) complexes of ligands **1**−**6** all cause the plasmid DNA to "disappear" during the incubation experiment at micromolar concentrations but do not generate any new DNA band or DNA smear (Figure 8). This is in stark

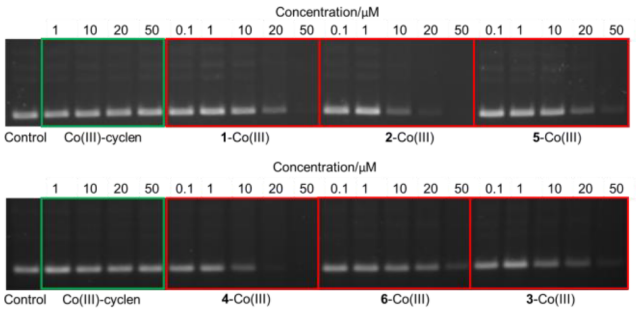

Figure 8. Cleavage experiment of (+) supercoiled pHOT-1 plasmid (0.007 $\mu g\ \mu L^{-1}$) in HEPES buffer (50 mM, pH 7.4) over 0.5 h.

contrast to Co(III)-cyclen itself, which has no effect whatsoever under these conditions. Interestingly, increasing the incubation time from 0.5 to 2 h had no significant effect on the results (Supplementary Figures S7 and S8), which suggests that the complete disappearance of DNA is caused by a binding event rather than multiple cleavage events. These data collectively suggest that the Co(III) complexes of ligands **1**−**6** possess significant hydrolytic DNase activity at micromolar concentrations but that the ligand−metal sequestering procedure used successfully for the Cu(II) complexes (see experimental procedures and Supplementary Figure S2) was unable to remove the Co(III) complexes from the DNA; presumably this in-turn (i) causes the DNA to be charge neutralized and consequently not to run on the gel or (ii) prevents the ethidium bromide from binding to the DNA.[43,44]

Indeed, Schneider[27] et al. notes that cleavage experiments with Co(III)-cyclen derivatives required cyanide treatment to sequester the cobalt prior to electrophoresis. Nonetheless, these data do demonstrate very clearly that the Co(III) complexes of the compounds **1**−**6** bind very strongly to DNA and therefore would not be able to generate a catalytic turnover. Presumably the Co(III) complexes of **1**−**6** form cyclic phosphate as the only hydrolysis product, which is known to be particularly stable for Co(III).[27] Consequently, the data suggest that such complexes could not operate as catalytic antibiotics on the ternary complex.

Cleavage in the Presence of Ascorbic Acid: Cu(II) Complexes. The Cu(II) complexes of ligands **1**−**6** in the presence of ascorbic acid all show very significant cleavage enhancement when compared with Cu(II)-cyclen; Figure 9 illustrates exemplar data for **2**-Cu(II) and **5**-Cu(II) (see Supplementary Figure S9 for the data of the other compounds). Presumably, the nuclease activity enhancement versus that of Cu(II)-cyclen is once again mediated by the extra binding affinity provided by the intercalation of the ciprofloxacin scaffold in **1**−**6** with the DNA. Interestingly, the concentration dependent conversion of form I to form II is similar for all the complexes but the conversion of form II to multiply nicked DNA (as evidenced by a DNA smear) varies considerably. The most active compound **2**-Cu(II) shows almost complete smearing of the DNA from 20 μM (see Figure 9), while **1**-Cu(II) shows only minimal smearing even at 40 μM (see Supplementary Figure S9). These data suggest that

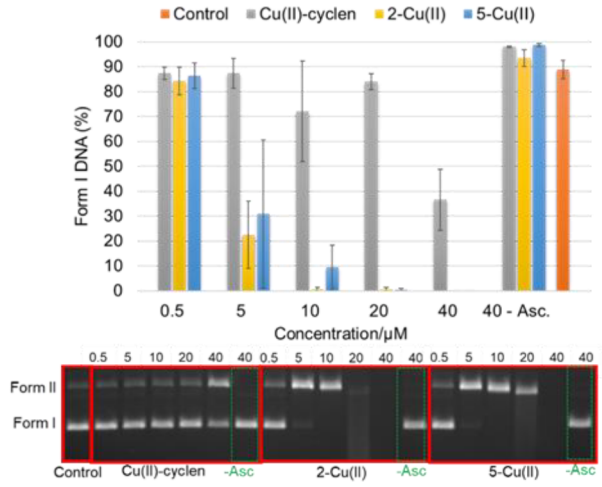

Figure 9. Concentration dependent cleavage of (+) supercoiled pHOT-1 plasmid (0.007 $\mu g\ \mu L^{-1}$) in HEPES buffer (50 mM, pH 7.4) and ascorbic acid (0.32 mM) over 2 h. "-Asc" = no ascorbate. Standard deviations of three independent experiments are shown as error bars. The agarose gel image shows one representative experiment.

while the cleavage ability of all the ligands is quite similar (i.e., k_2), the turnover frequency varies considerably.

To investigate the mechanism of cleavage, a scavenging assay was performed with hydroxyl radical scavengers (DMSO, *t*-BuOH, KI), a singlet oxygen scavenger (NaN_3), and a superoxide scavenger (KI) (Supplementary Figure S10). All the hydroxyl scavengers significantly inhibited the cleavage, NaN_3 showed no inhibition whatsoever, and KI did not show significantly more inhibition than DMSO or *t*-BuOH. These data suggest that in the presence of ascorbic acid, **5**-Cu(II) predominantly mediates DNA cleavage via the hydroxy radical mechanism.

***Escherichia coli* DNA Gyrase Assays.** To evaluate the biological effects and mechanism of the metal-free ligands **1**−**6** and their Cu(II) complexes on the topoisomerase IIA enzyme system (*in vitro*), two types of assays were performed: (i) an *E. coli* DNA gyrase supercoiling inhibition[45] assay (ATP-dependent[46]) and (ii) an *E. coli* DNA gyrase-induced DNA cleavage assay[47] (ATP-independent[48]).

Metal-free Ligands. The metal-free ligands **1**−**2** and **4**−**6** were tested for their in vitro activity in a gyrase inhibition[45] assay in which the supercoiling functionality of the enzyme was measured as a function of compound concentration in the presence of ATP, as exemplified by the results of **6** in Figure 10. The measured IC_{50} values (Table 1), demonstrate that the new compounds strongly inhibit DNA gyrase with a similar potency to the parent compound ciprofloxacin.

To investigate the mechanism of inhibition, a DNA gyrase-induced DNA cleavage assay[47] was performed in the absence of ATP. In this assay, the production of linear DNA from supercoiled DNA is measured as a function of compound concentration. Incubation of ciprofloxacin or the new compounds **1**−**6** with DNA gyrase, and DNA generates nicked DNA strands that are covalently linked to the active-site tyrosine residues of the enzyme DNA gyrase. Consequently, for the purposes of this assay, it is necessary to perform a second incubation of the reaction mixture with SDS and proteinase K, which enables the digestion of the DNA gyrase enzyme and thereby "frees" the linear DNA (form III) so that

https://dx.doi.org/10.1021/acsinfecdis.0c00777
ACS Infect. Dis. 2021, 7, 608−623

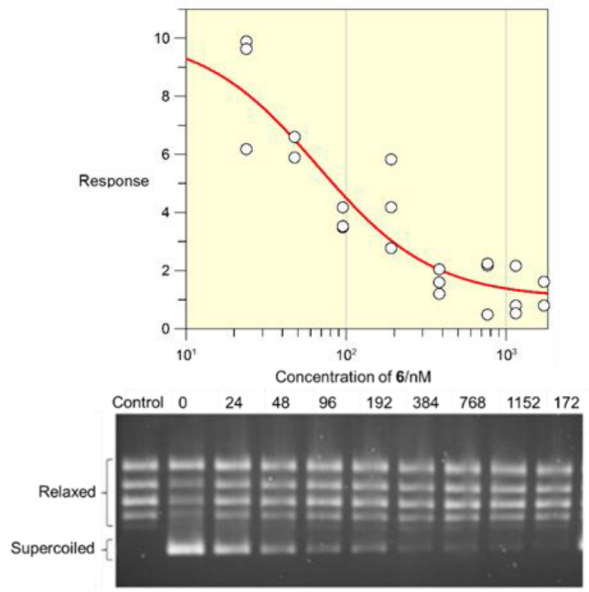

Figure 10. *E. coli* DNA gyrase was incubated with relaxed pHOT-1 plasmid (0.007 $\mu g\ \mu L^{-1}$) in Tris-HCl buffer (35 mM, pH 7.5) together with KCl (24 mM), $MgCl_2$ (4 mM), DTT (2 mM), spermidine (1.8 mM), 6.5% (w/v) glycerol, bovine serum albumin (0.1 mg/mL), ATP (1 mM), and various concentrations of compound **6**. The exemplar gel shows one example of the three independent experiments performed for compound **6**.

Table 1. MIC (μg/mL) and DNA Gyrase Inhibition (IC_{50}, μM) Values of Cipro and Compounds 1–6[a]

	bacterial MIC				
	Gram negative		Gram positive		
compound	*b*	*c*	*d*	*e*	IC_{50}
Cipro	0.05	0.05	0.19	0.02	0.11 ± 0.01
1	12	24	12	12	0.13 ± 0.03
1-Cu(II)	24	48	24	48	0.10 ± 0.01
1-Co(III)	12	12	24	12	-
2	12	6	12	12	0.24 ± 0.03
2-Cu(II)	12	6	12	12	0.24 ± 0.03
2-Cu(III)	12	6	24	12–24	-
3	24–48	12	6	6	-
3-Cu(II)	12	6	6	6	-
3-Co(III)	12	6	12–24	12	-
4	12–24	12–24	6–12	6–12	0.15 ± 0.01
4-Cu(II)	24	12	3	6	0.14 ± 0.02
4-Co(III)	12	6	6	6	-
5	*6*	*3*	*3*	*3*	*0.15 ± 0.04*
5-Cu(II)	6	6	6	3	0.18 ± 0.03
5-Co(III)	3	1.5	3	3	-
6	*3*	*1.5*	*1.5*	*3*	*0.07 ± 0.02*
6-Cu(II)	6	3	3	6	0.09 ± 0.01
6-Co(III)	6	3	3	3	-
$CuCl_2$	>384	>384	>384	>384	-

[a]The italic rows in the table highlight the most potent compounds. [b]*Escherichia coli* R477-100. [c]*Escherichia coli* 25922. [d]*Staphylococcus epidermidis*. [e]*Bacillus subtilis*.

it moves during electrophoresis. The tested compounds (**1**, **2**, and **4**) exhibited significant linearization of DNA (Supplementary Figure S11) but only after treatment with proteinase K, which demonstrates their ability to stabilize the ternary complex in a comparable manner to the parent compound ciprofloxacin.

Cu(II) Complexes. The Cu(II) complexes of ligands **1**, **2**, and **4**–**6** were initially tested in the DNA gyrase inhibition[45] assay; the measured IC_{50} data (Table 1) demonstrates that the Cu(II) complexes strongly inhibit DNA gyrase with a very similar potency to the metal-free ligands. To investigate the mechanism of inhibition, the DNA gyrase cleavage assay[47] was initially performed in the presence of proteinase K with compounds **1**-Cu(II), **2**-Cu(II), and **4**-Cu(II); as shown in Figure 11. All of these Cu(II) complexes linearized the DNA in a similar manner to the metal-free ligands in the presence of proteinase K.

The DNA gyrase cleavage assay was then performed without the proteinase K treatment, with ciprofloxacin, **1**-Cu(II), **2**-Cu(II), and **4**-Cu(II). It is highly noteworthy that, if these complexes do, in fact, cleave DNA, the ternary complex is likely to be destabilized and consequently lead to the release of linear DNA without needing to incubate with proteinase K, as schematically depicted in Figure 12. In this assay, **1**-Cu(II) was not able to generate linear DNA at any concentration, just like the parent compound ciprofloxacin. However, **4**-Cu(II) and to a lesser extent **2**-Cu(II) were able to generate a significant quantity of linear DNA and exhibited a well-defined, bell-shaped kinetic profile with a maximum at 25 μM (Figure 11). This is in stark contrast to the DNase activity of **4**-Cu(II) or **2**-Cu(II) on plasmid DNA (see Figure 6, Figure 9 and Supplementary Figure S9), which show concentration-dependent cleavage and no generation of linear DNA. Consequently, the observed data in Figure 11 demonstrate that both **4**-Cu(II) and **2**-Cu(II) indeed cleave DNA from within the ternary complex and subsequently cause it to become destabilized.

Vulnerability of Cu(II)-Cyclen under Physiological Conditions. While the above data with **4**-Cu(II) and **2**-Cu(II) can serve as a preliminary "proof of concept" for our design principles toward a catalytic fluoroquinolone, several questions remained unanswered. First, DNA cleavage experiments showed that two of the ingredients in the DNA gyrase cleavage assay, Tris-buffer and spermidine, both completely inhibit the hydrolytic DNA cleavage of plasmid DNA even for the most potent hydrolytic complex, **5**-Cu(II) (see Supplementary Figures S12 and S13); presumably a primary amine of Tris and of spermidine readily exchanges with the Cu(II)-associated water and thereby prevents the formation of the precatalytic complex between the DNA backbone and the Cu(II) complex (see Figure 3). However, **5**-Cu(II) was observed to retain significant oxidative cleavage activity in Tris buffer in the presence of the reducing agent DTT, an ingredient in the enzyme buffer (see Supplementary Figure S12). These data suggest that under the conditions of the DNA gyrase cleavage assay (Figure 11), the ternary complex destabilization effect of **4**-Cu(II) and **2**-Cu(II) is mediated solely by oxidative DNA cleavage and not by hydrolytic DNA cleavage.

Second, we were surprised by the similarity between the IC_{50} values for the metal-free and Cu(II) complexes of **2** and **4** (Table 1); since this assay (Figure 10), like the DNA gyrase-induced DNA cleavage assay (Figure 11) was performed in the presence of DTT, we expected these Cu(II) complexes to oxidatively cleave DNA from within the ternary complex and to thereby irreversibly inhibit (a significant proportion of) the DNA gyrase by covalently "trapping" the active site tyrosine to the DNA substrate (see Figure 12). This in-turn would be

https://dx.doi.org/10.1021/acsinfecdis.0c00777
ACS Infect. Dis. 2021, 7, 608–623

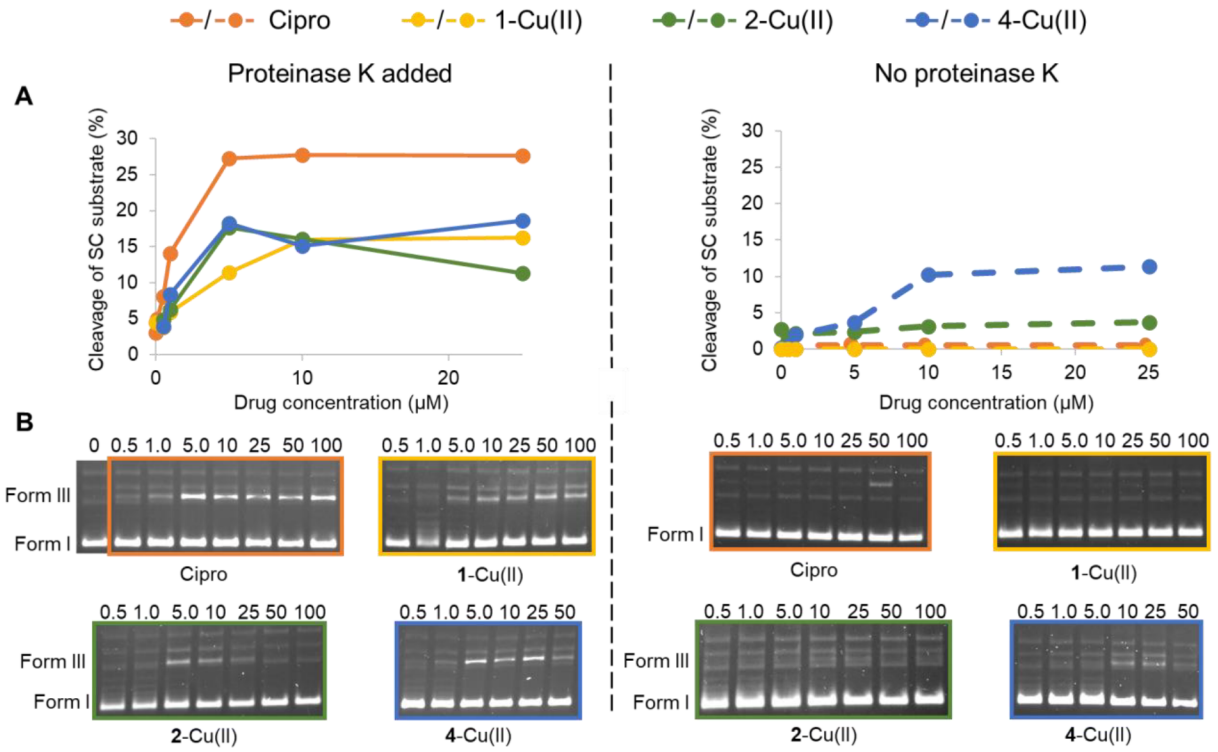

Figure 11. (A) Graphical representation of the exemplar data in part B for Cipro, **1**-Cu(II), **2**-Cu(II), and **4**-Cu(II). *E. coli* DNA gyrase was incubated with (+) supercoiled (SC) DNA (0.009 $\mu g\ \mu L^{-1}$) and various compounds using the same conditions as the supercoiling assay except for the absence of ATP. (B) Gels show the experiment for compounds **1**-Cu(II), **2**-Cu(II), and **4**-Cu(II) followed by additional incubation with proteinase K (left panel) and without proteinase K treatment (right panel).

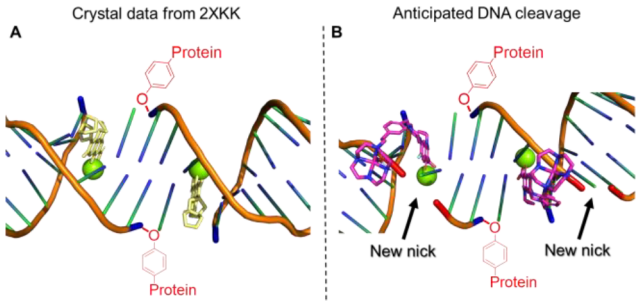

Figure 12. (A) Stabilization of the ternary complex by fluoroquinolone moxifloxacin (PDB ID code 2XKK). (B) Destabilization by catalytic cleavage of the DNA backbone by Cipro derivative **5**-Cu(II), prepared from docking results for **5**-Cu(II) in 2XKK (DNA = orange, Mg^{2+} = green, moxi = yellow, DNA gyrase tyrosine = red structural formula, **5**-Cu(II) = magenta).

expected to improve the inhibitory effect on DNA gyrase (i.e., to lower the IC_{50}).

Serendipitously, preliminary experiments that were being performed for a different assay (TopoIV-induced DNA cleavage assay[47]) revealed that ATP (one of the ingredients in the DNA gyrase supercoiling assay/Topo IV cleavage assay but not in the DNA gyrase cleavage assay) strongly inhibits both the hydrolytic and oxidative activity of the Cu(II) complexes of **1**−**6** (see Supplementary Figures S14 and S15), suggesting an explanation for the apparent lack of oxidative DNase activity in the gyrase supercoiling assay.

Furthermore, these experiments revealed that potassium glutamate (another ingredient of the Topo IV buffer) also strongly inhibits all DNase activity of the Cu(II) complexes of **1**−**6** (see Supplementary Figures S14 and S15). Subsequent UV−vis spectroscopic analysis of the mixture of Cu(II)-cyclen with potassium glutamate or ATP suggested that each of these ingredients inactivates the Cu(II)-cyclen warhead by displacement of the Cu(II)-associated water (see Supplementary Figures S16 and S17), thereby completely eliminating its potential DNase activity. Crucially, these results also provide an explanation for the unexpected similarity between the MIC data (see below) for the Cu(II) complexes of **2** and **4** and their corresponding metal-free ligands (see Table 1), since free ATP and glutamate are present in bacterial cells at concentrations comparable to the enzyme buffer.[49,50]

In summary, the observed data encouragingly suggests that at least two of the compounds (i.e., **4**-Cu(II) and **2**-Cu(II)) are in principle (i.e., *in vitro*) able to fragment the bacterial chromosome into linear DNA in the presence of bacterial topoisomerase IIA enzyme via DNA cleavage and subsequent destabilization of the ternary complex. However, the data also demonstrates the "vulnerability" of the Cu(II)-cyclen system *in vivo*, since (i) the natural amino acids along with other substances containing primary amines and (ii) endogenous metal chelators such as ATP and glutamate would all have the potential to bind and inactivate the Cu(II)-cyclen moiety. In fact, to some extent, these findings are potentially relevant to any metallodrug that has not lived up to its promise *in vivo*, since by definition the metal center must leave coordination sites available for its interaction with the biological target,[51,52] which also makes it vulnerable toward unwanted ligand exchange reactions.[53] To address this issue for the Cu(II)-cyclen system, it would be interesting to explore the potential of a dynamic, intramolecular cap in the so-called "second coordination sphere".[54] Such dynamic ligand exchange systems could facilitate DNA cleavage catalysis[55] but also prevent

https://dx.doi.org/10.1021/acsinfecdis.0c00777
ACS Infect. Dis. 2021, 7, 608−623

irreversible ligand exchange reactions, thereby ensuring the integrity of the Cu(II)-cyclen catalytic system even in a biological setting.

Antibacterial Activity. Encouraged by the above data, we then tested the compounds **1**−**6** and their Cu(II) and Co(III) complexes for their comparative antibacterial activity by determining MIC values against two Gram-negative *E. coli* strains (R477-100 and 25922) and two Gram-positive strains, *Staphylococcus epidermidis* and *Bacillus subtilis*. The observed data (Table 1) show that all the new derivatives of ciprofloxacin exhibit significant antibacterial activity against Gram-negative and Gram-positive bacteria. The derivatives **5** and **6** (with aromatic linker) show slightly higher activity in comparison to the rest of the compounds against all the tested bacteria.

However, the new compounds have significantly reduced antibacterial activity relative to the parent ciprofloxacin. To rule out the possibility that alternative antimicrobial susceptibility testing procedures are necessary for these positively charged compounds, several modifications that have been reported to significantly impact the MIC values of various cationic antibacterial peptides were investigated: (i) the growth medium was changed from the Luria−Bertani medium to the Mueller−Hinton medium,[56,57] (ii) BSA was added into the growth medium (12% w/v),[58] or (iii) the polypropylene 96-well plates were replaced with glass tubes.[59] Unfortunately, none of these modifications significantly changed the observed MIC values. The discrepancy between the *ex vivo* (MIC) and *in vitro* (IC_{50}) data suggests that the cellular permeability of the synthetic compounds is significantly lower than that of the parent drug or the compounds have increased offsite binding, both of which could be attributed to the high polarity of the cyclen moiety. Indeed, a very similar reduction in antibacterial potency of ciprofloxacin derivatives was also observed when it was conjugated with other highly positively charged substances like aminoglycosides to yield hybrid antibiotics.[45,60,61]

Furthermore, all the Cu(II) and Co(III) complexes of **1**−**6** exhibit similar antibacterial activity compared to the corresponding compounds without the metal ion, corroborating the IC_{50} data for the Cu(II) complexes (Table 1) and the DNA cleavage assay data for Co(III) complexes (Figure 8). However, when the MIC was determined in the presence of a high concentration of DTT (10 mM), **4**-Cu(II) showed significantly improved antibacterial activity (8-fold) against *E. coli* R477-100 (MIC values of 3.0 and 24 μg/mL, respectively, with and without DTT), while $CuCl_2$ and **1**-Cu(II) showed no change whatsoever under the same conditions. Furthermore, a similar trend (4-fold improvement) was observed for **4**-Cu(II) against another *E. coli* strain (25922) and against another bacterial species (*B. subtilis*). These data corroborate the findings of the DNA gyrase cleavage assay (see Figures 11 and 12) and provide an *ex vivo* proof of concept. Presumably, the high concentration of DTT is able to compete effectively with endogenous Cu(II)-cyclen poisons such as ATP and glutamate, thereby facilitating the oxidative DNase activity of **4**-Cu(II) even under "vulnerabilizing" cellular conditions.

SUMMARY AND CONCLUSIONS

In this study, the concept of catalytic antibiotics was examined by redesigning the fluoroquinolone ciprofloxacin that exhibits broad spectrum antibacterial activity by targeting the bacterial type IIA topoisomerase enzymes. Metal−cyclen complexes (Cu(II)-cyclen and Co(III)-cyclen) were chosen as potential catalytic warheads, covalently attached to the ciprofloxacin scaffold through different lengths of aliphatic (compounds **1**−**3**) and aromatic (compounds **4**−**6**) linkers. These compounds were rationally designed to cleave DNA from within the ternary complex using X-ray crystallographic data from the literature and molecular docking.

The Cu(II) and Co(III) complexes of six new derivatives of ciprofloxacin (compounds **1**−**6**) were synthesized and evaluated *in vitro* for their ability (i) to inhibit the bacterial DNA gyrase activity and (ii) to cleave plasmid DNA in the presence or absence of the gyrase enzyme and *ex vivo* for their antibacterial activity.

We found that the *in vitro* DNase activity of the Cu(II) complexes of ligands **1**−**6** in the absence of type IIA topoisomerase enzymes was concentration-dependent and significantly higher than that of the Cu(II)-cyclen itself, under both hydrolytic and oxidative conditions. The observed hydrolytic activity correlated strongly with linker length, while the oxidative activity varied more indiscriminately as expected. The observed data also demonstrated that the Co(III) complexes are more active than the corresponding Cu(II) complexes of the designer structures. However, the Co(III) complexes showed exceedingly enhanced binding to plasmid DNA, suggesting that these complexes would be unable to generate a catalytic turnover.

The new designer compounds **1**−**6** and their Cu(II) complexes showed good antibacterial activity against both Gram-negative and Gram-positive bacteria and proved to be highly potent bacterial DNA gyrase inhibitors, exhibiting very similar inhibition potencies for both the metal-free and Cu(II) complexes of ligands **1**−**6** in comparison to that of the parent ciprofloxacin (Table 1). Furthermore, the DNA gyrase cleavage assays showed that both the metal-free and Cu(II) complexes of ligands inhibit these enzymes by stabilizing the ternary complex like the parent ciprofloxacin. These observations demonstrate that the binding mode and the subsequent antibacterial mechanism of action of the parent ciprofloxacin scaffold are retained within the new designer structures **1**−**6** and their Cu(II) complexes. Furthermore, (i) **2**-Cu(II) and **4**-Cu(II) were shown to generate linear DNA under oxidative conditions (with DTT), in the presence of DNA gyrase without the addition of proteinase K, and (ii) **4**-Cu(II) demonstrated significantly enhanced antibacterial activity in the presence of a high concentration of DTT, thereby demonstrating a proof of concept *in vitro* and *ex vivo*, respectively. It was also shown, however, that both the hydrolytic and oxidative activity of the Cu(II)-ligand complexes are completely inhibited under "normal" cellular conditions due to ligand exchange, which explains why the MIC (Table 1, without DTT) and IC_{50} values of all the Cu(II)-ligands are essentially the same as the metal-free ligands. Consequently, these data demonstrate the vulnerability of the Cu(II)-cyclen system and in fact highlight the general issue of undesired *in vivo* ligand exchange as a potential challenge for any prospective metallodrug.

In summary, this pilot study provides insights into the challenges and potential solutions of designing novel, metal-based, ciprofloxacin−nuclease molecules that target the topoisomerase IIA bacterial enzymes via a catalytic mechanism. Furthermore, it demonstrates the importance of considering whether a "protective umbrella" needs to be incorporated into the second coordination sphere of any metallodrug to ensure the integrity of the active species.

https://dx.doi.org/10.1021/acsinfecdis.0c00777
ACS Infect. Dis. 2021, 7, 608−623

METHODS

General. ^{1}H and ^{13}C NMR, DEPT, COSY, HMQC, and HMBC spectra were recorded on a Bruker AvanceTM 600/500/400/300 spectrometers. Chemical shifts reported (in ppm) are relative to $CHCl_3$ (δ = 7.26) with $CDCl_3$ as the solvent, to HOD or internal MeOH (δ = 4.79) with D_2O as the solvent, and to CD_3OH (δ = 3.31) with MeOH as the solvent. Mass spectral analyses were performed on a Bruker Maxis Impact under electron spray ionization (ESI+) QTOFMS or on a Thermo LCQ fleet under electron spray ionization (ESI+). Reactions were monitored by TLC on silica gel (Gel 60 F254, 0.25 mm, Merck), and spots were visualized by UV lamp, iodine, or charring with a yellow solution containing $(NH_4)_6Mo_7O_{24}{\cdot}4H_2O$ (120 g) and $(NH_4)_2Ce(NO_3)_6$ (5 g) in 10% H_2SO_4 (800 mL). Flash column chromatography was performed on silica gel 60 (70−230 mesh). The EPR spectra were recorded on a Bruker EMX-10/12 X-band (ν = 9.3 GHz) digital EPR spectrometer. The spectra were recorded at a microwave power of 200 mW, 100 kHz, magnetic field modulation of 3 G amplitude. Digital field resolution was 2048 points per spectrum. Spectral processing and simulation were performed with the Bruker WIN-EPR and SimFonia Software. The UV−vis spectra were recorded on an Ultrospec 2100 pro spectrometer. Analytical HPLC was performed on Thermo Dionex UltiMate 3000, using a Phenomenex C18 column and a detection wavelength of 271 nm. All chemicals unless otherwise stated were obtained from commercial sources. Purity of the final conjugates **1**−**6** and their Cu(II) salts were determined by using HPLC analysis, which indicated >95% purity unless otherwise stated (see Supporting Information).

Removal of Ligands prior to Electrophoresis. The procedure proved to be necessary (see Supplementary Figure S2) when more than 100 μM Cu(II)−ligand complex was employed, that is, (only) for the DNA cleavage assays that were performed in the absence of any adjuvants. An Amberlyst 15 (Sigma-Aldrich) ion-exchange resin was prepared according to the reported literature[27] and stored at −20 °C. Directly before use, 0.5 g of the exchanger was mixed with 250 μL of water. After stopping the DNA-cleavage reaction by addition of EDTA (54 mM, 15 min incubation at 37 °C), 10 μL of the exchanger suspension was added, vortexed, and incubated at 37 °C for 15 min before centrifugation and electrophoresis.

DNA Cleavage Assays. DNA cleavage activity of complexes **1**−**6** toward supercoiled (+) pHOT-1 plasmid DNA (TopoGEN) was monitored by gel electrophoresis. In a typical experiment, plasmid DNA (200 ng, 0.007 μg mL^{-1}) in HEPES buffer (50 mM, pH 7.4) was mixed with different concentrations of metal complexes **1**−**6** in the presence or absence of ascorbic acid (0.32 mM). All stock solutions of buffers and of complexes **1**−**6** were prepared using HPLC grade water (ChromAR). Molecular biology reagent grade water (Sigma) was added up to a total reaction volume of 30 μL before incubation for a given time. For the ascorbic acid assays, the reaction was quenched immediately after incubation with EDTA (54 mM). For analysis, 10 μL of loading buffer (40% sucrose, 100 mM Tris.HCl (pH 7.5), 1 mM EDTA, 0.5 mg mL^{-1} bromophenol blue) was added to the incubated solution, and the mixture was loaded onto an agarose (SeaKem LE) gel [1% in TAE × 1 buffer (40 mM Tris, 20 mM acetic acid, 1 mM EDTA)]. Electrophoresis was carried out at 60 V for 2 h. Gels were stained with 1 μg mL^{-1} ethidium bromide for 30 min and destained in TAE × 1 buffer. DNA bands were visualized with medium-range ultraviolet light using Bio-Rad Gel Doc XR+ imaging system. The quantity of different DNA forms (I or II) was estimated using ImageJ[62] software.

***E. coli* Gyrase DNA Supercoiling Assay.** The DNA supercoiling reactions were based on the manufacturer protocol (TopoGEN). The amount of DNA gyrase used in each assay was optimized by testing various dilutions of the stock. The amount sufficient to supercoil 250 ng of the substrate in 1 h at 37 °C was then used for the testing of compounds (1.1 U as defined by manufacturer). Assays (30 μL) contained 250 ng of relaxed pHOT1 plasmid DNA in Tris-HCl buffer (35 mM), pH 7.5, containing KCl (24 mM), $MgCl_2$ (4 mM), DTT (2 mM), spermidine (1.8 mM), ATP (1 mM), 6.5% (w/v) glycerol, and bovine serum albumin (0.1 mg/mL). Reactions were incubated at 37 °C for 60 min. Reaction mixtures were stopped by the addition of 30 μL of loading buffer (40% sucrose, 100 mM Tris·HCl (pH 7.5), 1 mM EDTA, 0.5 mg mL^{-1} bromophenol blue) and worked up using 30 μL of 24:1 chloroform/isoamyl alcohol mixture; the aqueous layer was then analyzed using electrophoresis. Electrophoresis, gel staining, DNA visualization, and DNA quantification were performed as described for the DNA cleavage assays. The IC_{50} value was defined as the drug concentration that reduced the enzymatic activity observed with drug-free controls by 50% using nonlinear regression, three parameter curve fit using GraFit 5[63] software.

***E. coli* Gyrase DNA Cleavage Assay.** *E. coli* gyrase enzyme was purchased from TopoGEN, and the DNA cleavage reactions were based on the protocol of Inspiralis. Assays (30 μL) contained supercoiled (+) pHOT1 plasmid (200 ng) and DNA gyrase (5 U as defined by manufacturer) in 35 mM Tris-HCl (pH 7.5), 24 mM KCl, 4 mM $MgCl_2$, 2 mM DTT, 1.8 mM spermidine, 6.5% (w/v) glycerol, and 0.1 mg/mL bovine serum albumin. Reactions were incubated at 37 °C for 60 min. Enzyme−DNA cleavage complexes were trapped by adding 3 μL of 2% SDS. Following this, 1.5 μL of 10 mg/mL proteinase K (Sigma-Aldrich) was added (where relevant), and the reaction mixtures were incubated at 37 °C for 30 min to digest the gyrase enzyme. Samples were mixed with 30 μL of loading buffer (40% sucrose, 100 mM Tris-HCl (pH 7.5), 1 mM EDTA, 0.5 mg mL^{-1} bromophenol blue) and worked up using 30 μL of 24:1 chloroform/isoamyl alcohol mixture; the aqueous layer was then analyzed using electrophoresis. Electrophoresis, gel staining, DNA visualization, and DNA quantification were performed as described for the DNA cleavage assays. DNA double stranded cleavage was monitored by the conversion of supercoiled plasmid to linear DNA and quantified in comparison to a control drug-free reaction.

Antibacterial Activity. Comparative antibacterial activities were determined by measuring the MIC values using the double-microdilution method according to the National Committee for Clinical Laboratory Standards[64] (NCCLS). Luria−Bertani growth medium and polypropylene 96-well plates (Thermo) were used unless otherwise stated. All the experiments were performed in triplicate, and analogous results were obtained in three different experiments.

Synthesis. *Compound 7.* Dowex 50 WX8 ion-exchange resin (mesh 200−400, 27 g) was set stirring with commercially available ciprofloxacin (10 g, 0.03 mol) in MeOH (500 mL) and refluxed under an argon atmosphere. TLC analysis [a mixture of MeOH/DCM/$MeNH_2$ (33% in ethanol) in a ratio 10:10:0.5] indicated almost complete consumption of the

https://dx.doi.org/10.1021/acsinfecdis.0c00777
ACS Infect. Dis. 2021, 7, 608−623

starting material after 48 h. The crude reaction mixture was neutralized with 25% $NH_4OH_{(aq)}$ at 0 °C, transferred to a sintered glass column, and then washed extensively with 25% $NH_4OH_{(aq)}$ until all of the product had been eluted. The solvent was then evaporated to yield a white solid (8.4 g, 24.3 mmol, 81%); ^{1}H NMR (300 MHz, $CDCl_3$) δ_H 8.52 (s, 1H, quinolone *H-2*), 8.02 (d, J_{HF} = 13.4 Hz, 1H, QH-5), 7.25 (d, J_{HF} = 7.1 Hz, 1H, QH-8), 3.90 (s, 3H, OCH_3), 3.47−3.37 (m, 1H, cyclopropane CH), 3.27−3.18 (m, 4H, piperazine 2 × CH_2), 3.13−3.04 (m, 4H, piperazine 2 × CH_2), 1.35−1.26 (m, 2H, cyclopropane CH_2), 1.16−1.08 (m, 2H, cyclopropane CH_2); ^{13}C NMR (126 MHz, $CDCl_3$) δ_C 173.02 (d, J_{CF} = 2.2 Hz, C═O), 166.18 (s, C═O), 152.69 (d, J_{CF} = 248.8 Hz, Ar), 148.31 (s, C−H Ar), 144.28 (d, J_{CF} = 10.8 Hz, Ar), 137.96 (d, J_{CF} = 0.9 Hz, Ar), 122.05 (d, J_{CF} = 7.6 Hz, Ar), 112.32 (d, J_{CF} = 21.0 Hz, C−H Ar), 109.72 (s, C−H Ar), 104.19 (d, J_{CF} = 3.3 Hz, C−H Ar), 51.98 (s, OCH_3), 50.35 (d, J_{CF} = 4.4 Hz, piperazine CH_2), 45.91 (s, piperazine CH_2), 34.59 (s, cyclopropane CH), 8.12 (s, cyclopropane CH_2). ESI+ QTOFMS calculated for $C_{18}H_{21}FN_3O_3$ ($[M + H]^+$) *m/e* 346.15; measured *m/e* 346.10.

General Procedure for the Synthesis of 8a−d. To a stirring suspension of **7** and *N*,*N*-diisopropylethylamine (DIPEA) (4 equiv) in CH_3CN (35 mL/gram of **7**) was added the appropriate dibromo compound (10 equiv) under an atmosphere of argon and set stirring at 60 °C overnight. TLC analysis (DCM/MeOH 9:1) indicated complete consumption of **7** after 20 h. The solvent was evaporated, and the residue dried in vacuo overnight. The crude product was then loaded onto a DCM-packed silica column as a DCM solution; the desired product was eluted in 3% MeOH/DCM to yield **8a−d** as white solids. Chemical yields of **8a−d** and their complete analytical data are given in the Supporting Information.

General Procedure for the Synthesis of 8e,f. A suspension of **7** and DIPEA (4 equiv) in CH_3CN (35 mL/gram of **7**) was set stirring in an ice bath, and then the appropriate dibromo compound (**10** or **11**) was added (1.2 equiv) under an atmosphere of argon. The ice-bath was maintained for the duration of the reaction. TLC analysis (DCM/MeOH 9:1) indicated complete consumption of **7** after 12 h. The solvent was evaporated, and the residue was dried in vacuo overnight. The crude product was then loaded onto a DCM-packed silica column as a DCM solution; the desired product was eluted in 3% MeOH/DCM to yield **8e,f** as white solids. Chemical yields of **8e,f** and their complete analytical data are given in the Supporting Information.

General Procedure for the Synthesis of 9a−c and 9e,f. *Step 1.* The appropriate bromo derivative (**8a−c,e,f**), free-amine form of cyclen[37] (2 equiv) and Cs_2CO_3 (2.2 equiv) were added to dry CH_3CN (35 mL/gram of bromo derivative) to form a suspension and set stirring under an argon atmosphere. The reaction mixture was then heated to 60 °C. TLC analysis (DCM/MeOH/25% $NH_4OH_{(aq)}$ 15:3:0.3) indicated complete consumption of the bromo derivative after 20 h (it should be noted that the unwanted elimination product of **8e** appears at the same R_f as the starting material). The reaction mixture was filtered, the residue was washed extensively with CH_3CN, and then the filtrate was evaporated in vacuo.

Step 2. The crude from the previous step and Et_3N (10 equiv) were dissolved in dry DCM (35 mL/g of bromo derivative) and set stirring in an ice bath under an argon atmosphere. Boc_2O (10 equiv) was then added. The reaction mixture was allowed to rise to room temperature. TLC analysis (DCM/MeOH 9:1) indicated complete consumption of the starting material (the *N*-alkylated intermediate from step 1) after 15 h. The solvent was evaporated, and the residue was dried in vacuo overnight. The crude product was then loaded onto a DCM-packed silica column as a DCM solution; the desired product was eluted in a solvent mixture of MeOH and DCM to yield **9a−c** and **9e,f** as white solids. Chemical yields of **9a−c** and **9e,f** and their complete analytical data are given in the Supporting Information.

Compound 9d. Compound **8d** (410 mg, 0.78 mmol), tri-Boc-cyclen[36] (660 mg, 1.40 mmol), and DIPEA (0.4 mL, 2.34 mmol) were dissolved in dry DCM (40 mL). The reaction mixture was set stirring at room temperature. TLC analysis (DCM/MeOH 15:1) indicated complete consumption of the bromo derivative after 2 weeks. The solvent was evaporated, and then the residue was dried in vacuo overnight. The crude product was loaded onto a DCM-packed silica column as a DCM solution; the desired product was eluted in DCM/MeOH gradient from 35:1 to 30:1 to yield **9d** as a white solid (520 mg, 0.57 mmol, 72%). The complete analytical data of **9d** is given in the Supporting Information.

General Procedure for the Synthesis of 1−6. *Step 1.* The appropriate derivative (**9a−f**) was dissolved in a mixture of MeOH and H_2O (5:1, 65 mL/gram of starting material). An aqueous solution of LiOH (5 equiv) was then added, and the reaction mixture was stirred at room temperature. TLC analysis (15:1 DCM/MeOH and 25:1:1 DCM/MeOH/25% $NH_4OH_{(aq)}$) indicated complete consumption of the starting material after 20 h. The solvents were then evaporated, followed by workup with diethyl ether and brine. The desired product was isolated in the organic phase, which was dried with $MgSO_4$ and then evaporated to yield a white solid.

Step 2. The crude from the previous step was dissolved in a mixture of TFA and DCM (1:1, 30 mL/g of derivative **9a−f**) and set stirring at room temperature. TLC analysis (15:15:10:5 MeOH/DCM/$MeNH_2$ [33 wt % in ethanol]/H_2O and 10:10:5 MeOH/DCM/25% $NH_4OH_{(aq)}$) indicated complete consumption of the starting material after 15 h. The TFA and DCM were evaporated, and then the residue was dried in vacuo overnight. The dry crude was then dissolved in water, neutralized with $NaHCO_3$(aq), and then loaded onto an Amberlite CG50 (H^+-form, 100−200 mesh) column. The column was washed sequentially with H_2O, MeOH, MeOH/H_2O, and then once again H_2O. The desired product was then eluted using a mixture of 2.5% $NH_4OH_{(aq)}$, MeOH, and H_2O in a ratio of 1:3:6, respectively. The solvent was then evaporated to yield **1−6** as white solids.

Compound 1. Following the general procedure, compound **9a** (542 mg, 0.6 mmol) yielded 48% over 2 steps (167 mg, 0.29 mmol); ^{1}H NMR (500 MHz, CD_3OD) δ_H 8.64 (s, 1H, QH-2), 7.94 (d, J_{HF} = 13.6 Hz, 1H, QH-5), 7.49 (d, J_{HF} = 7.3 Hz, 1H, QH-8), 3.67−3.60 (m, 1H, cyclopropane CH), 3.32−3.27 (m, 4H, piperazine 2 × CH_2), 2.93−2.86 (m, 12H, cyclen 6 × CH_2), 2.70 (t, *J* = 5.2 Hz, 4H, cyclen 2 × CH_2), 2.59−2.54 (m, 4H, piperazine 2 × CH_2), 2.52 (t, *J* = 7.4 Hz, 2H, linker CH_2-cyclen), 2.18 (t, *J* = 8.1 Hz, 2H, linker CH_2-piperazine), 1.48 (quint, *J* = 7.5 Hz, 2H, linker CH_2), 1.43−1.32 (m, 4H, cyclopropane CH_2, linker CH_2), 1.24 (quint, *J* = 7.5 Hz, 2H, linker CH_2), 1.19−1.10 (m, 4H, cyclopropane CH_2, linker CH_2); ^{13}C NMR (126 MHz, CD_3OD) δ_C 176.75 (s, C═O), 172.34 (s, C═O), 154.62 (d, J_{CF} = 247.8 Hz, Ar), 148.61 (s,

https://dx.doi.org/10.1021/acsinfecdis.0c00777
ACS Infect. Dis. 2021, 7, 608−623

C−H Ar), 145.95 (d, J_{CF} = 10.8 Hz, Ar), 140.23 (s, Ar), 123.19 (d, J_{CF} = 6.6 Hz, Ar), 116.59 (s, Ar), 113.04 (d, J_{CF} = 23.1 Hz, C−H Ar), 106.64 (s, C−H Ar), 59.77 (s, linker CH_2-piperazine), 55.19 (s, linker CH_2-cyclen), 54.12 (s, piperazine CH_2), 51.37 (s, cyclen CH_2), 50.70 (d, J_{CF} = 3.7 Hz, piperazine CH_2), 46.63 (s, cyclen CH_2), 44.99 (s, cyclen CH_2), 44.75 (s, cyclen CH_2), 35.83 (s, cyclopropane CH), 28.80 (s, linker CH_2), 28.64 (s, linker CH_2), 28.17 (s, linker CH_2), 27.64 (s, linker CH_2), 8.54 (s, cyclopropane CH_2). HRMS (ESI+ QTOFMS) calculated for $C_{31}H_{48}FN_7O_3$ ($[M + H]^+$) *m/e* 586.3875; measured *m/e* 586.3900.

Compound **2**. Following the general procedure, compound **9b** (511 mg, 0.56 mmol) yielded 41% over 2 steps (140 mg, 0.23 mmol); ^{1}H NMR (500 MHz, CD_3OD) δ_H 8.60 (s, 1H, QH-2), 7.92 (d, J_{HF} = 13.1 Hz, 1H, QH-5), 7.45 (d, J_{HF} = 7.1 Hz, 1H, QH-8), 3.62−3.54 (m, 1H, cyclopropane CH), 3.35−3.28 (m, 4H, piperazine 2 × CH_2), 2.82−2.76 (m, 4H, cyclen 2 × CH_2), 2.73−2.67 (m, 8H, piperazine 2 × CH_2, cyclen 2 × CH_2), 2.66−2.61 (m, 4H, cyclen 2 × CH_2), 2.61−2.56 (m, 4H, cyclen 2 × CH_2), 2.49−2.40 (m, 4H, linker CH_2-piperazine, linker CH_2-cyclen), 1.60−1.54 (m, 2H, linker CH_2), 1.52−1.46 (m, 2H, linker CH_2), 1.39−1.31 (m, 8H, cyclopropane CH_2, linker 3 × CH_2), 1.16−1.10 (m, 2H, cyclopropane CH_2); ^{13}C NMR (126 MHz, CD_3OD) δ_C 176.95 (s, C═O), 172.66 (s, C═O), 154.52 (d, J_{CF} = 246.9 Hz, Ar), 148.64 (s, C−H Ar), 145.73 (d, J_{CF} = 11.1 Hz, Ar), 139.99 (s, Ar), 123.53 (s, Ar), 117.58 (s, Ar), 113.10 (d, J_{CF} = 23.4 Hz, C−H Ar), 106.42 (s, C−H Ar), 59.77 (s, linker CH_2-piperazine), 55.36 (s, linker CH_2-cyclen), 54.14 (s, piperazine CH_2), 52.17 (s, cyclen CH_2), 50.75 (d, J_{CF} = 4.3 Hz, piperazine CH_2), 47.16 (s, cyclen CH_2), 46.02 (s, cyclen CH_2), 45.20 (s, cyclen CH_2), 35.63 (s, cyclopropane CH), 30.61 (s, linker CH_2), 28.70 (s, linker CH_2), 28.63 (s, linker CH_2), 28.45 (s, linker CH_2), 27.52 (s, linker CH_2), 8.48 (s, cyclopropane CH_2). HRMS (ESI+ QTOFMS) calculated for $C_{32}H_{51}FN_7O_3$ ($[M + H]^+$) *m/e* 600.4032; measured *m/e* 600.4007.

Compound **3**. Following the general procedure, compound **9c** (1.06 g, 1.14 mmol) yielded 61% over 2 steps (430 mg, 0.70 mmol); ^{1}H NMR (500 MHz, CD_3OD) δ_H 8.60 (s, 1H, QH-2), 7.91 (d, J_{HF}= *12.9 Hz*, 1H, QH-5), 7.49 (d, J_{HF}= *7.2 Hz*, 1H, QH-8), 3.67−3.58 (m, 1H, cyclopropane CH), 3.36−3.30 (m, 4H, piperazine 2 × CH_2), 2.94−2.79 (m, 12H, cyclen 6 × CH_2), 2.74−2.59 (m, 8H, piperazine 2 × CH_2, cyclen 2 × CH_2), 2.47 (t, *J* = *7.2 Hz*, 2H, linker CH_2-cyclen), 2.34 (t, *J* = 7.9 Hz, 2H, linker CH_2-piperazine), 1.50−1.39 (m, 4H, linker 2 × CH_2), 1.39−1.32 (m, 2H, cyclopropane CH_2), 1.23−1.10 (m,10H, cyclopropane CH_2, linker 4 × CH_2); ^{13}C NMR (126 MHz, CD_3OD) δ_C 176.61 (s, C═O), 172.35 (s, C═O), 154.54 (d, J_{CF} = 247.2 Hz, Ar), 148.41 (s, C−H Ar), 145.85 (d, J_{CF} = 10.6 Hz, Ar), 140.12 (s, Ar), 123.29 (s, Ar), 117.06 (s, Ar), 113.03 (d, C−H Ar), 106.58 (s, J_{CF} = 2.4 Hz, C−H Ar), 59.85 (s, linker CH_2-piperazine), 55.14 (s, linker CH_2-cyclen), 54.18 (s, piperazine CH_2), 51.34 (s, cyclen CH_2), 50.76 (d, J_{CF} = 4.2 Hz, piperazine CH_2), 46.57 (s, cyclen CH_2), 45.01 (s, cyclen CH_2), 44.67 (s, cyclen CH_2), 35.74 (s, cyclopropane CH), 30.84 (s, linker CH_2), 30.83 (s, linker CH_2), 28.77 (s, linker CH_2), 28.61 (s, linker CH_2), 27.99 (s, linker CH_2), 27.62 (s, linker CH_2), 8.54 (s, cyclopropane CH_2). HRMS (ESI+ QTOFMS) calculated for $C_{33}H_{53}FN_7O_3$ ($[M + H]^+$) *m/e* 614.4188; measured *m/e* 614.4145.

Compound **4**. Following the general procedure, compound **9d** (697 mg, 0.76 mmol) yielded 50% over 2 steps (232 mg, 0.38 mmol); NMR analysis is of TFA salt. ^{1}H NMR (500 MHz, D_2O) δ_H 8.67 (s, 1H, QH-2), 7.61 (d, *J* = 7.9 Hz, 2H, linker Ar), 7.56 (d, J_{HF}= 12.8 Hz, 1H, QH-5), 7.54−7.50 (m, 3H, QH-8, linker Ar), 4.51 (s, 2H, linker CH_2-piperazine), 4.01−3.89 (m, 4H, piperazine CH_2, linker CH_2-cyclen), 3.76−3.66 (m, 3H, piperazine CH_2, cyclopropane CH), 3.51−3.42 (m, 2H, piperazine CH_2), 3.39−3.13 (m, 10H, piperazine CH_2, cyclen 4 × CH_2), 3.07−2.95 (m, 4H, cyclen 2 × CH_2), 2.92 (t, *J* = 5.1 Hz, 4H, cyclen 2 × CH_2), 1.45−1.39 (m, 2H, cyclopropane CH_2), 1.23−1.17 (m, 2H, cyclopropane CH_2); ^{13}C NMR (126 MHz, D_2O) δ_C 176.08 (s, C═O), 169.01 (s, C═O), 162.69 (s, C═O of TFA), 153.34 (d, J_{CF} = 251.3 Hz, Ar), 148.39 (s, C−H Ar), 144.04 (d, J_{CF} = 10.7 Hz, Ar), 138.95 (s, Ar), 137.08 (s, linker Ar), 131.69 (s, C−H linker Ar), 130.67 (s, C−H linker Ar), 127.83 (s, linker Ar), 118.99 (d, J_{CF} = 8.0 Hz, Ar), 116.24 (q, J_{CF} = 292.4 Hz, CF_3 of TFA), 110.73 (d, J_{CF} = 23.5 Hz, C−H Ar), 106.72 (s, C−H Ar), 105.70 (s, Ar), 59.92 (s, linker CH_2-piperazine), 55.83 (s, linker CH_2-cyclen), 50.91 (s, piperazine CH_2), 47.30 (s, cyclen CH_2), 46.33 (d, J_{CF} = 3.8 Hz, piperazine CH_2), 44.21 (s, cyclen CH_2), 41.79 (s, cyclen CH_2), 41.56 (s, cyclen CH_2), 36.05 (s, cyclopropane CH), 7.37 (s, cyclopropane CH_2). HRMS (ESI+ QTOFMS) calculated for $C_{33}H_{45}FN_7O_3$ ($[M + H]^+$) *m/e* 606.3562; measured *m/e* 606.3583.

Compound **5**. Following the general procedure, compound **9e** (857 mg, 0.92 mmol) yielded 38% over 2 steps (214 mg, 0.35 mmol); ^{1}H NMR (500 MHz, CD_3OD) δ_H 8.58 (s, 1H, QH-2), 7.88 (d, J_{HF}= 13.5 Hz, 1H, QH-5), 7.38 (d, J_{HF} = 7.0 Hz, 1H, QH-8), 7.16 (d, *J* = 7.6 Hz, 2H, linker Ar), 7.08 (d, *J* = 7.6 Hz, 2H, linker Ar), 3.55−3.50 (m, 1H, cyclopropane CH), 3.49 (bs, 2H, linker CH_2-piperazine), 3.29−3.22 (m, 4H, piperazine 2 × CH_2), 2.86−2.80 (m, 4H, cyclen 2 × CH_2), 2.80−2.74 (m, 8H, cyclen 4 × CH_2), 2.74−2.66 (m, 8H, cyclen 2 × CH_2, linker CH_2CH_2-cyclen, linker CH_2CH_2-cyclen), 2.63−2.57 (m, 4H, piperazine 2 × CH_2), 1.31−1.24 (m, 2H, cyclopropane CH_2), 1.11−1.02 (m, 2H, cyclopropane CH_2); ^{13}C NMR (126 MHz, CD_3OD) δ_C 176.71 (s, C═O), 172.44 (s, C═O), 154.51 (d, J_{CF} = 247.4 Hz, Ar), 148.39 (s, C−H Ar), 145.83 (d, J_{CF} = 10.6 Hz, Ar), 140.61 (s, linker Ar), 140.02 (s, Ar), 135.95 (s, linker Ar), 130.85 (s, C−H linker Ar), 129.74 (s, C−H linker Ar), 123.25 (s, Ar), 117.35 (s, Ar), 113.03 (d, J_{CF} = 22.1 Hz, C−H Ar), 106.50 (s, C−H Ar), 63.55 (s, linker CH_2-piperazine), 56.81 (s, linker CH_2CH_2-cyclen), 53.86 (s, piperazine CH_2), 51.30 (s, cyclen CH_2), 50.88 (d, J_{CF} = 4.0 Hz, piperazine CH_2), 46.64 (s, cyclen CH_2), 45.13 (s, cyclen CH_2), 44.87 (s, cyclen CH_2), 35.67 (s, cyclopropane CH), 33.87 (s, linker CH_2CH_2−cyclen), 8.51 (s, cyclopropane CH_2). HRMS (ESI+ QTOFMS) calculated for $C_{34}H_{47}FN_7O_{32}$ ($[M + H]^+$) 620.3719 *m/e*; measured *m/e* 620.3687.

Compound **6**. Following the general procedure, compound **9f** (1.32 g, 1.39 mmol) yielded 59% over 2 steps (519 mg, 0.82 mmol); ^{1}H NMR (500 MHz, CD_3OD) δ_H 8.59 (s, 1H, QH-2), 7.87 (d, J_{HF} = 13.5 Hz, 1H, QH-5), 7.44 (d, J_{HF} = 7.3 Hz, 1H, QH-8), 7.06 (d, *J* = 7.9 Hz, 2H, linker Ar), 6.99 (d, *J* = 7.9 Hz, 2H, linker Ar), 3.61−3.53 (m, 1H, cyclopropane CH), 3.43 (bs, 2H, linker CH_2-piperazine), 3.30−3.23 (m, 4H, piperazine 2 × CH_2), 2.90−2.80 (m, 12H, cyclen 6 × CH_2), 2.70−2.64 (m, 4H, cyclen 2 × CH_2), 2.60−2.54 (m, 4H, piperazine 2 × CH_2), 2.53−2.45 (m, 4H, linker CH_2(CH_2)$_2$−cyclen, linker (CH_2)$_2$CH_2-cyclen), 1.80−1.68 (m, 2H, linker CH_2CH_2CH_2−cyclen), 1.36−1.25 (m, 2H, cyclopropane CH_2), 1.15−1.06 (m, 2H, cyclopropane CH_2); ^{13}C NMR (126 MHz, CD_3OD)

https://dx.doi.org/10.1021/acsinfecdis.0c00777
ACS Infect. Dis. 2021, 7, 608−623

δ_C 176.64 (s, C═O), 172.27 (s, C═O), 154.56 (d, J_{CF} = 247.9 Hz, Ar), 148.31 (s, C−H Ar), 145.94 (d, J_{CF} = 10.5 Hz, Ar), 142.38 (s, linker Ar), 140.11 (s, Ar), 135.62 (s, linker Ar), 130.52 (s, C−H linker Ar), 129.26 (s, C−H linker Ar), 123.09 (d, J_{CF} = 6.4 Hz, Ar), 116.92 (s, Ar), 113.02 (d, J_{CF} = 23.1 Hz, C−H Ar), 106.53 (d, J_{CF} = 2.9 Hz, C−H Ar), 63.60 (s, linker CH_2-piperazine), 54.96 (s, linker $(CH_2)_2CH_2$-cyclen), 53.89 (s, piperazine CH_2), 51.55 (s, cyclen CH_2), 50.87 (d, J_{CF} = 3.9 Hz, piperazine CH_2), 46.72 (s, cyclen CH_2), 45.09 (s, cyclen CH_2), 44.87 (s, cyclen CH_2), 35.76 (s, cyclopropane CH), 34.25 (s, linker $CH_2(CH_2)_2$−cyclen), 29.72 (s, linker $CH_2CH_2CH_2$−cyclen), 8.53 (s, cyclopropane CH_2). HRMS (ESI+ QTOFMS) calculated for $C_{35}H_{49}FN_7O_3$ ($[M + H]^+$) m/e 634.3875; measured m/e 634.3877.

General Procedure for the Synthesis and Characterization of Aqua Cu(II) Complexes. A stoichiometric amount of $CuCl_{2(aq)}$ (1.0 equiv) was added to an aqueous solution of the cyclen derivative (compounds **1**−**6**, 10 mg in 1 mL), and the mixture was set stirring at room temperature. UV−vis spectroscopy (λ_{max} 600 nm) was used to follow the progress of the complexation until completion. The solution was then microfiltered and lyophilized to produce the desired complex in quantitative yield. The complexes were characterized by UV−vis, HRMS, and EPR. The EPR spectra of the Cu(II) complexes of the cyclen derivatives **1**−**6** were identical and comparable with the simulated spectra and with the literature values for Cu(II)-cyclen.[65] The solid state (liquid nitrogen) demonstrated the expected axial symmetry with $g_{parallel}$ = 2.171 and $g_{perpendicular}$ = 2.070 [$A_{parallel}(^{63,65}Cu)$ = 175.0 G]. In water solution, Cu(II) is characterized by the interaction of an unpaired electron with the magnetic isotopes of copper [$a(^{63,65}Cu)$ = 73.0 G, (I = 3/2) and a g-factor that is strongly shifted (g_{iso} = 2.104) from that of a free-electron value (2.0023) (see Supporting Information for EPR spectra). Chemical yields of Cu(II)Cl_2 complexes of ligands **1**−**6** and their analytical data are given in the Supporting Information.

General Procedure for the Synthesis and Characterization of Aqua-Hydroxo Co(III) Complexes. The syntheses followed the reported literature[38] procedure with slight changes and included the following three steps:

Step 1: Synthesis of Co(III)CO_3 Complexes as Demonstrated by the Synthesis of cis-[Co(cyclen)CO_3]HCO_3. Free-amine cyclen (0.070 g, 0.406 mmol) was dissolved in a MeOH/H_2O mixture (1:1, 2 mL) and an equimolar amount of $Na_3[Co(CO_3)_3]\cdot 3H_2O$ (0.147 g, 0.406 mmol) was added. The dark green solution was left to react for 16 h at 65 °C. The solution was filtered while hot under gravity to separate the liquid from a black solid. The filtrate was dried in vacuo and redissolved in MeOH (4 mL), and the resulting solution was filtered to remove a white precipitate. The resulting filtrate was dried in vacuo, redissolved in water and then lyophilized to afford a pink powder (0.071 g, 50%). ^{1}H NMR (500 MHz, D_2O) δ_H = 3.60−3.48 (m, 2H, CH_2), 3.15−3.06 (m, 2H, CH_2), 3.02−2.89 (m, 4H, 2 × CH_2), 2.88−2.80 (m, 6H, 3 × CH_2), 2.77−2.68 (m, 2H, CH_2); ^{13}C NMR (126 MHz, D_2O with internal MeOH marker) δ = 171.66 (s), 167.24 (s), 162.34 (s) (free HCO_3^-, free CO_3^{2-}, complexed CO_3^{2-}), 56.37 (s, CH_2), 53.92 (s, CH_2), 50.40 (s, CH_2), 47.79 (s, CH_2); UV/vis (H_2O) λ_{max} = 517, 362 nm; ESI+ QTOFMS calculated for $C_9H_{20}CoN_4O_3$ ($[M]^+$) 291.09 m/e; measured 291.11 m/e.

The Co(III)CO_3 complexes of ligands **1**−**6** were characterized by UV−vis, ^{13}C NMR, and MS. The ^{13}C NMR peaks of the cyclen carbons of the complexes were significantly shifted from the metal-free ligands as observed for the Co(III)-cyclen complex itself; this clearly demonstrated that the Co(III) had become coordinated to the cyclen group as desired. Chemical yields of Co(III)CO_3 complexes of ligands **1**−**6** and their analytical data are given in the Supporting Information.

Steps 2 and 3: Synthesis and Activation of Co(III)Cl_2 Complexes as Demonstrated by the Synthesis and Activation of cis-[Co(cyclen)Cl_2]Cl. *cis*-[Co(cyclen)CO_3]-HCO_3 (0.071 g, 0.270 mmol) was dissolved in MeOH (3 mL), and then HCl (10.2 M, 1.5 mL) was added gradually. The reaction mixture was reduced to dryness in vacuo, and the residue was again dissolved in MeOH (3 mL), treated with HCl (10.2 M, 1.5 mL), and then reduced to dryness. This procedure was repeated once more, and a gradual color change from dark pink to dark violet was observed. The dry residue was then redissolved in MeOH (5 mL) and placed into an ice bath, and then ether was added (45 mL). The resulting precipitate was filtered under gravity using a sintered glass funnel and then washed multiple times with ether until the filtrate was pH-neutral to afford a violet solid in quantitative yield. ^{13}C NMR (126 MHz, D_2O with internal MeOH marker) δ = 57.34 (s, CH_2), 54.21 (s, CH_2), 49.60 (s, CH_2), 46.23 (s, CH_2); UV/vis (DMSO) λ_{max} = 560, 380 nm. A 5 mM stock solution of the dichloride complex was prepared in HEPES (10 mM, pH 7.6) and then activated to the catalytically active aqua-hydroxo species by addition of 2 equiv of 0.1 M NaOH at room temperature, as shown by the immediate change in the visible absorption band from 560 to 519 nm.

The Co(III)Cl_2 complexes of ligands **1**−**6** were characterized by UV−vis and HRMS. Chemical yields of Co(III)Cl_2 complexes of ligands **1**−**6** and their analytical data are given in the Supporting Information.

■ ASSOCIATED CONTENT

Supporting Information

The Supporting Information is available free of charge at https://pubs.acs.org/doi/10.1021/acsinfecdis.0c00777.

Supplementary schemes and figures, synthetic and analytical data for compounds **8a**−**f**, **9a**−**f**, **10a**, **10**, **11a**−**c**, and **11**, ^{1}H and ^{13}C NMR spectra of compounds **1**−**6**, synthetic and analytical data for Cu(II) and Co(III) complexes of **1**−**6**, and molecular docking data (PDF)

■ AUTHOR INFORMATION

Corresponding Author

Timor Baasov − *Edith and Joseph Fischer Enzyme Inhibitors Laboratory, Schulich Faculty of Chemistry, Technion − Israel Institute of Technology, Haifa 3200003, Israel;* orcid.org/0000-0002-1427-2619; Email: chtimor@technion.ac.il

Authors

Moshe N. Goldmeier − *Edith and Joseph Fischer Enzyme Inhibitors Laboratory, Schulich Faculty of Chemistry, Technion − Israel Institute of Technology, Haifa 3200003, Israel*

Sofya Katz − *Edith and Joseph Fischer Enzyme Inhibitors Laboratory, Schulich Faculty of Chemistry, Technion − Israel Institute of Technology, Haifa 3200003, Israel*

https://dx.doi.org/10.1021/acsinfecdis.0c00777
ACS Infect. Dis. 2021, 7, 608−623

Fabian Glaser − *The Lorry I. Lokey Interdisciplinary Center for Life Sciences and Engineering, Technion - Israel Institute of Technology, Haifa 3200003, Israel*
Valery Belakhov − *Edith and Joseph Fischer Enzyme Inhibitors Laboratory, Schulich Faculty of Chemistry, Technion − Israel Institute of Technology, Haifa 3200003, Israel*
Alina Khononov − *Edith and Joseph Fischer Enzyme Inhibitors Laboratory, Schulich Faculty of Chemistry, Technion − Israel Institute of Technology, Haifa 3200003, Israel*

Complete contact information is available at: https://pubs.acs.org/10.1021/acsinfecdis.0c00777

Author Contributions

T.B. and M.N.G. conceived and designed the research. M.N.G. and S.K. performed most experimental work and data analysis. V.B. performed parts of the synthetic work, A.K. performed parts of the biological work, and F.G. performed parts of the molecular docking and simulations. T.B. and M.N.G. wrote the manuscript. All authors approved the final version.

Funding

This work was supported by research grants from the Israel Science Foundation founded by the Israel Academy of Sciences and Humanities (grant nos. 1845/14, 670/20, for T.B.). V.B. acknowledges financial support by the Ministry of Immigration Absorption and the Ministry of Science and Technology, Israel (Kamea Program).

Notes

The authors declare no competing financial interest.

■ ACKNOWLEDGMENTS

We acknowledge Dr. Boris Tumansky for his assistance with the acquisition and interpretation of EPR spectra and Dr. Guy Kamnesky for running HPLC analysis.

■ ABBREVIATIONS

ATCUN, amino terminal copper and nickel; Topo IV, topoisomerase IV; cyclen, 1,4,7,10-tetraazacyclododecane; DIPEA, *N*,*N*-diisopropylethylamine

■ REFERENCES

(1) Dalhoff, A. (2012) Resistance Surveillance Studies: A Multifaceted Problem-the Fluoroquinolone Example. *Infection 40* (3), 239−262.
(2) Drlica, K., Malik, M., Kerns, R. J., and Zhao, X. (2008) Quinolone-Mediated Bacterial Death. *Antimicrob. Agents Chemother. 52* (2), 385−392.
(3) Aldred, K. J., Kerns, R. J., and Osheroff, N. (2014) Mechanism of Quinolone Action and Resistance. *Biochemistry 53* (10), 1565−1574.
(4) Charrier, C., Salisbury, A. M., Savage, V. J., Duffy, T., Moyo, E., Chaffer-Malam, N., Ooi, N., Newman, R., Cheung, J., Metzger, R., McGarry, D., Pichowicz, M., Sigerson, R., Cooper, I. R., Nelson, G., Butler, H. S., Craighead, M., Ratcliffe, A. J., Best, S. A., and Stokes, N. R. (2017) Novel Bacterial Topoisomerase Inhibitors with Potent Broad-Spectrum Activity against Drug-Resistant Bacteria. *Antimicrob. Agents Chemother. 61* (5), e02100-16.
(5) Pokrovskaya, V., Nudelman, I., Kandasamy, J., and Baasov, T. (2010) Aminoglycosides. *Methods Enzymol. 478*, 437−462.
(6) Yu, Z., and Cowan, J. A. (2017) Catalytic Metallodrugs: Substrate-Selective Metal Catalysts as Therapeutics. *Chem. - Eur. J. 23* (57), 14113−14127.
(7) Singh, J., Petter, R. C., Baillie, T. A., and Whitty, A. (2011) The Resurgence of Covalent Drugs. *Nat. Rev. Drug Discovery 10* (4), 307−317.
(8) Suh, J. (2014) Progress in Designing Artificial Proteases: A New Therapeutic Option for Amyloid Diseases. *Asian J. Org. Chem. 3* (1), 18−32.
(9) Mancin, F., Scrimin, P., and Tecilla, P. (2012) Progress in Artificial Metallonucleases. *Chem. Commun. 48* (45), 5545−5559.
(10) Joyner, J. C., Hodnick, W. F., Cowan, A. S., Tamuly, D., Boyd, R., and Cowan, J. A. (2013) Antimicrobial Metallopeptides with Broad Nuclease and Ribonuclease Activity. *Chem. Commun. 49* (21), 2118−2120.
(11) Alexander, J. L., Thompson, Z., Yu, Z., and Cowan, J. A. (2019) Cu-ATCUN Derivatives of Sub5 Exhibit Enhanced Antimicrobial Activity via Multiple Modes of Action. *ACS Chem. Biol. 14* (3), 449−458.
(12) Libardo, M. D. J., Bahar, A. A., Ma, B., Fu, R., McCormick, L. E., Zhao, J., McCallum, S. A., Nussinov, R., Ren, D., Angeles-Boza, A. M., and Cotten, M. L. (2017) Nuclease Activity Gives an Edge to Host-Defense Peptide Piscidin 3 over Piscidin 1, Rendering It More Effective against Persisters and Biofilms. *FEBS J. 284* (21), 3662−3683.
(13) Libardo, M. D. J., De La Fuente-Nuñez, C., Anand, K., Krishnamoorthy, G., Kaiser, P., Pringle, S. C., Dietz, C., Pierce, S., Smith, M. B., Barczak, A., Kaufmann, S. H. E., Singh, A., and Angeles-Boza, A. M. (2018) Phagosomal Copper-Promoted Oxidative Attack on Intracellular Mycobacterium Tuberculosis. *ACS Infect. Dis. 4* (11), 1623−1634.
(14) Wang, T.-Y., Libardo, M. D. J., Angeles-Boza, A. M., and Pellois, J.-P. (2017) Membrane Oxidation in Cell Delivery and Cell Killing Applications. *ACS Chem. Biol. 12* (5), 1170−1182.
(15) Smolkin, B., Khononov, A., Pieńko, T., Shavit, M., Belakhov, V., Trylska, J., and Baasov, T. (2019) Towards Catalytic Antibiotics: Redesign of Aminoglycosides To Catalytically Disable Bacterial Ribosomes. *ChemBioChem 20* (2), 247−259.
(16) Bax, B. D., Murshudov, G., Maxwell, A., and Germe, T. (2019) DNA Topoisomerase Inhibitors: Trapping a DNA-Cleaving Machine in Motion. *J. Mol. Biol. 431* (18), 3427−3449.
(17) Wohlkonig, A., Chan, P. F., Fosberry, A. P., Homes, P., Huang, J., Kranz, M., Leydon, V. R., Miles, T. J., Pearson, N. D., Perera, R. L., Shillings, A. J., Gwynn, M. N., and Bax, B. D. (2010) Structural Basis of Quinolone Inhibition of Type IIA Topoisomerases and Target-Mediated Resistance. *Nat. Struct. Mol. Biol. 17* (9), 1152−1153.
(18) (2017) *The PyMOL Molecular Graphics System*, version 2.0.4, Schrödinger, LLC.
(19) Wolfenden, R. (2006) Degrees of Difficulty of Water-Consuming Reactions in the Absence of Enzymes. *Chem. Rev. 106* (8), 3379−3396.
(20) Cleland, W. W., and Hengge, A. C. (2006) Enzymatic Mechanisms of Phosphate and Sulfate Transfer. *Chem. Rev. 106* (8), 3252−3278.
(21) Dupureur, C. M. (2008) Roles of Metal Ions in Nucleases. *Curr. Opin. Chem. Biol. 12* (2), 250−255.
(22) Yu, Z., and Cowan, J. (2018) Metal Complexes Promoting Catalytic Cleavage of Nucleic Acids — Biochemical Tools and Therapeutics. *Curr. Opin. Chem. Biol. 43*, 37−42.
(23) Alkhader, S., Ezra, A., Kasparkova, J., Brabec, V., and Yavin, E. (2010) A Metal-Free DNA Nuclease Based on a Cyclic Peptide Scaffold. *Bioconjugate Chem. 21* (8), 1425−1431.
(24) Veyrier, F. J., and Cellier, M. F. (2015) Metal Economy in Host-Microbe Interactions. *Front. Cell. Infect. Microbiol. 4*, 190.
(25) Hancock, R. D., Salim Shaikjee, M., Dobson, S. M., and Boeyens, J. C. A. (1988) The Stereochemical Activity or Non-Activity of the "Inert" Pair of Electrons on Lead(II) in Relation to Its Complex Stability and Structural Properties. Some Considerations in Ligand Design. *Inorg. Chim. Acta 154* (2), 229−238.
(26) Joyner, J. C., Reichfield, J., and Cowan, J. A. (2011) Factors Influencing the DNA Nuclease Activity of Iron, Cobalt, Nickel, and Copper Chelates. *J. Am. Chem. Soc. 133* (39), 15613−15626.

(27) Hettich, R., and Schneider, H.-J. (1997) Cobalt(III) Polyamine Complexes as Catalysts for the Hydrolysis of Phosphate Esters and of DNA. A Measurable 10 Million-Fold Rate Increase. *J. Am. Chem. Soc. 119* (24), 5638−5647.
(28) Page, M. I., and Jencks, W. P. (1971) Entropic Contributions to Rate Accelerations in Enzymic and Intramolecular Reactions and the Chelate Effect. *Proc. Natl. Acad. Sci. U. S. A. 68* (8), 1678−1683.
(29) Lee, T. Y., and Suh, J. (2009) Target-Selective Peptide-Cleaving Catalysts as a New Paradigm in Drug Design. *Chem. Soc. Rev. 38* (7), 1949−1957.
(30) Greenwood, N. N., and Earnshaw, A. (1997) *Chemistry of the Elements*, 2nd ed., p 1123, Butterworth-Heinemann, Oxford.
(31) Hubschwerlen, C., Specklin, J.-L., Sigwalt, C., Schroeder, S., and Locher, H. H. (2003) Design, Synthesis and Biological Evaluation of Oxazolidinone−Quinolone Hybrids. *Bioorg. Med. Chem. 11* (10), 2313−2319.
(32) Kerns, R. J., Rybak, M. J., Kaatz, G. W., Vaka, F., Cha, R., Grucz, R. G., and Diwadkar, V. U. (2003) Structural Features of Piperazinyl-Linked Ciprofloxacin Dimers Required for Activity against Drug-Resistant Strains of Staphylococcus Aureus. *Bioorg. Med. Chem. Lett. 13* (13), 2109−2112.
(33) Zhang, X., Liu, X., Phillips, D. L., and Zhao, C. (2016) Mechanistic Insights into the Factors That Influence the DNA Nuclease Activity of Mononuclear Facial Copper Complexes Containing Hetero-Substituted Cyclens. *ACS Catal. 6* (1), 248−257.
(34) Morris, G. M., Huey, R., Lindstrom, W., Sanner, M. F., Belew, R. K., Goodsell, D. S., and Olson, A. J. (2009) Software News and Updates AutoDock4 and AutoDockTools4: Automated Docking with Selective Receptor Flexibility. *J. Comput. Chem. 30* (16), 2785−2791.
(35) Zhao, H., and Caflisch, A. (2013) Discovery of ZAP70 Inhibitors by High-Throughput Docking into a Conformation of Its Kinase Domain Generated by Molecular Dynamics. *Bioorg. Med. Chem. Lett. 23* (20), 5721−5726.
(36) Kimura, E., Aoki, S., Koike, T., and Shiro, M. (1997) A Tris(Zn II −1,4,7,10-Tetraazacyclododecane) Complex as a New Receptor for Phosphate Dianions in Aqueous Solution. *J. Am. Chem. Soc. 119* (13), 3068−3076.
(37) Athey, P. S., and Kiefer, G. E. (2002) A New, Facile Synthesis of 1,4,7,10-Tetraazacyclododecane: Cyclen. *J. Org. Chem. 67* (12), 4081−4085.
(38) Jorge, A. R., Chernobryva, M., Rigby, S. E. J., Watkinson, M., and Resmini, M. (2016) Incorporation of Cobalt-Cyclen Complexes into Templated Nanogels Results in Enhanced Activity. *Chem. - Eur. J. 22* (11), 3764−3774.
(39) Hormann, J., van der Meer, M., Sarkar, B., and Kulak, N. (2015) From Cyclen to 12-Crown-4 Copper(II) Complexes: Exchange of Donor Atoms Improves DNA Cleavage Activity. *Eur. J. Inorg. Chem. 2015* (28), 4722−4730.
(40) Kashiba-Iwatsuki, M., Yamaguchi, M., and Inoue, M. (1996) Role of Ascorbic Acid in the Metabolism of *S* -Nitroso-Glutathione. *FEBS Lett. 389* (2), 149−152.
(41) Liu, Q., Zhang, J., Wang, M. Q., Zhang, D. W., Lu, Q.-S., Huang, Y., Lin, H. H., and Yu, X. Q. (2010) Synthesis, DNA Binding and Cleavage Activity of Macrocyclic Polyamines Bearing Mono- or Bis-Acridine Moieties. *Eur. J. Med. Chem. 45* (11), 5302−5308.
(42) Zhang, Y., Huang, Y., Zhang, J., Zhang, D., Liu, J., Liu, Q., Lin, H., and Yu, X. (2011) Synthesis, DNA Binding and Cleavage Studies of the Copper(II) Complexes of PNA-Cyclen Conjugates. *Sci. China: Chem. 54* (1), 129−136.
(43) Hormann, J., Malina, J., Lemke, O., Hülsey, M. J., Wedepohl, S., Potthoff, J., Schmidt, C., Ott, I., Keller, B. G., Brabec, V., and Kulak, N. (2018) Multiply Intercalator-Substituted Cu(II) Cyclen Complexes as DNA Condensers and DNA/RNA Synthesis Inhibitors. *Inorg. Chem. 57* (9), 5004−5012.
(44) Rocha, M. S., Cavalcante, A. G., Silva, R., and Ramos, E. B. (2014) On the Effects of Intercalators in DNA Condensation: A Force Spectroscopy and Gel Electrophoresis Study. *J. Phys. Chem. B 118*, 4832.
(45) Pokrovskaya, V., Belakhov, V., Hainrichson, M., Yaron, S., and Baasov, T. (2009) Design, Synthesis, and Evaluation of Novel Fluoroquinolone-aminoglycoside Hybrid Antibiotics. *J. Med. Chem. 52* (8), 2243−2254.
(46) Gellert, M., Mizuuchi, K., O'Dea, M. H., and Nash, H. A. (1976) DNA Gyrase: An Enzyme That Introduces Superhelical Turns into DNA. *Proc. Natl. Acad. Sci. U. S. A. 73* (11), 3872−3876.
(47) Luan, G., and Drlica, K. (2018) Fluoroquinolone-Gyrase-DNA Cleaved Complexes. *Methods Mol. Biol. 1703*, 269−281.
(48) Ashley, R. E., Dittmore, A., Mcpherson, S. A., Turnbough, C. L., Neuman, K. C., and Osheroff, N. (2017) Activities of Gyrase and Topoisomerase IV on Positively Supercoiled DNA. *Nucleic Acids Res. 45* (16), 9611−9624.
(49) Richey, B., Cayley, D. S., Mossing, M. C., Kolka, C., Anderson, C. F., Farrar, T. C., and Record, M. T. (1987) Variability of the Intracellular Ionic Environment of Escherichia Coli. Differences between in Vitro and in Vivo Effects of Ion Concentrations on Protein-DNA Interactions and Gene Expression. *J. Biol. Chem. 262* (15), 7157−7164.
(50) Yaginuma, H., Kawai, S., Tabata, K. V., Tomiyama, K., Kakizuka, A., Komatsuzaki, T., Noji, H., and Imamura, H. (2015) Diversity in ATP Concentrations in a Single Bacterial Cell Population Revealed by Quantitative Single-Cell Imaging. *Sci. Rep. 4* (1), 1−7.
(51) Barreto, J., Joshi, T., Venkatachalam, T., Reutens, D. C., Graham, B., and Spiccia, L. (2015) Coordination Chemistry of a Mono-Dibenzofuran Derivative of 1,4,7,10-Tetraazacyclododecane. *J. Coord. Chem. 68* (2), 335−349.
(52) Joshi, T., Graham, B., and Spiccia, L. (2015) Macrocyclic Metal Complexes for Metalloenzyme Mimicry and Sensor Development. *Acc. Chem. Res. 48* (8), 2366−2379.
(53) Mjos, K. D., and Orvig, C. (2014) Metallodrugs in Medicinal Inorganic Chemistry. *Chem. Rev. 114* (8), 4540−4563.
(54) Zhao, M., Wang, H. B., Ji, L. N., and Mao, Z. W. (2013) Insights into Metalloenzyme Microenvironments: Biomimetic Metal Complexes with a Functional Second Coordination Sphere. *Chem. Soc. Rev. 42* (21), 8360−8375.
(55) Tjioe, L., Joshi, T., Forsyth, C. M., Moubaraki, B., Murray, K. S., Graham, B., Spiccia, L., and Brugger, J. (2012) Phosphodiester Cleavage Properties of Copper(II) Complexes of 1,4,7-Triazacyclononane Ligands Bearing Single Alkyl Guanidine Pendants. *Inorg. Chem. 51*, 939.
(56) Giacometti, A., Cirioni, O., Barchiesi, F., Del Prete, M. S., Fortuna, M., Caselli, F., and Scalise, G. (2000) In Vitro Susceptibility Tests for Cationic Peptides: Comparison of Broth Microdilution Methods for Bacteria That Grow Aerobically. *Antimicrob. Agents Chemother. 44* (6), 1694−1696.
(57) Mercer, D. K., Torres, M. D. T., Duay, S. S., Lovie, E., Simpson, L., von Köckritz-Blickwede, M., de la Fuente-Nunez, C., O'Neil, D. A., and Angeles-Boza, A. M. (2020) Antimicrobial Susceptibility Testing of Antimicrobial Peptides to Better Predict Efficacy. *Front. Cell. Infect. Microbiol. 10*, 326.
(58) Oesterreicher, Z., Eberl, S., Nussbaumer-Proell, A., Peilensteiner, T., and Zeitlinger, M. (2019) Impact of Different Pathophysiological Conditions on Antimicrobial Activity of Glycopeptides in Vitro. *Clin. Microbiol. Infect. 25* (6), 759.
(59) Ezadi, F., Ardebili, A., and Mirnejad, R. (2019) Antimicrobial Susceptibility Testing for Polymyxins: Challenges, Issues, and Recommendations. *J. Clin. Microbiol. 57* (4), e01390-18.
(60) Pokrovskaya, V., and Baasov, T. (2010) Dual-Acting Hybrid Antibiotics: A Promising Strategy to Combat Bacterial Resistance. *Expert Opin. Drug Discovery 5* (9), 883−902.
(61) Shavit, M., Pokrovskaya, V., Belakhov, V., and Baasov, T. (2017) Covalently Linked Kanamycin − Ciprofloxacin Hybrid Antibiotics as a Tool to Fight Bacterial Resistance. *Bioorg. Med. Chem. 25* (11), 2917−2925.
(62) Schneider, C. A., Rasband, W. S., and Eliceiri, K. W. (2012) NIH Image to ImageJ: 25 Years of Image Analysis. *Nat. Methods 9* (7), 671−675.

https://dx.doi.org/10.1021/acsinfecdis.0c00777
ACS Infect. Dis. 2021, 7, 608−623

(63) Leatherbarrow, R. J. (2001) *GraFit 5*, Erithacus Software Ltd., Horley, U.K.
(64) NCCLS (1994) *National Committee for Clinical Laboratory Standards, Performance Standards for Antimicrobial Susceptibility Testing. Fifth Information Supplement: Approved Standard M100-S5*, NCCLS, Villanova, PA.
(65) Sawada, T., Fukumaru, K., and Sakurai, H. (1995) L-Band ESR Spectra of Copper(II) Complexes with CuN4 Configurations. *Biochem. Biophys. Res. Commun. 216* (1), 154−161.

https://dx.doi.org/10.1021/acsinfecdis.0c00777
ACS Infect. Dis. 2021, 7, 608−623